Publisher's version: Tousignant, K. & Packer, J. A. (2017). Numerical investigation of fillet welds in HSS-to-rigid end-plate connections, Journal of Structural Engineering, American Society of Civil Engineers 143(12): 04017165-1 – 04017165-16.
https://doi.org/10.1061/(ASCE)ST.1943-541X.0001889

NUMERICAL INVESTIGATION OF FILLET WELDS IN HSS-TO-RIGID END-PLATE CONNECTIONS

Kyle Tousignant[1], B.A.Sc

Jeffrey A. Packer[2*], Ph.D., D.Sc., P.Eng., F.ASCE

[1] Ph.D. Candidate, Department of Civil Engineering, University of Toronto, 35 St. George Street, Toronto, ON, M5S 1A4, Canada.

[2] Bahen/Tanenbaum Professor, Department of Civil Engineering, University of Toronto, 35 St. George Street, Toronto, ON, M5S 1A4, Canada.

* Corresponding author:

Phone: +1-416-978-4776

Fax: +1-416-978-7046

E-mail: jeffrey.packer@utoronto.ca

ABSTRACT

This paper presents a finite element (FE) investigation on the behavior of fillet-welded hollow structural section (HSS) rigid end-plate connections, wherein the entire weld length is effective. The FE models are validated by comparison to 33 experimental tests and a parametric study is then performed with 73 numerical tests to evaluate the effect of weld size, HSS branch wall slenderness and branch inclination angle, on fillet weld strength. The inherent problem with one-sided fillet welds to a tension-loaded element is illustrated. A reliability analysis determined that the directional strength-increase factor for fillet welds in North America leads to inadequate values of the safety index for joints to both circular and rectangular HSS, especially for connections with large welds. Hence, an alternative yet safe method for estimating the strength of fillet welds to HSS, based on weld size, is proposed. An expression for the fillet weld size required to develop the yield strength of a 90° HSS branch member is derived.

Keywords: hollow structural section, rectangular hollow section, circular hollow section, connection, joint, welding, directional strength-increase factor, fillet weld, finite element.

INTRODUCTION

When proportioning welds to resist the applied forces in axially-loaded branch members of hollow structural section (HSS) connections, weld effective lengths are required (ISO, 2013). Weld effective lengths account for the non-uniform loading of the weld due to differences in the relative flexibility of the HSS chord face, around the weld perimeter. Weld effective lengths for truss connections between rectangular hollow sections (RHS) have been researched at the University of Toronto over the last several decades by Frater and Packer (1992a, 1992b), Packer and Cassidy (1995), McFadden and Packer (2014), and Tousignant and Packer (2015). AISC 360 Section K5 (AISC 2016), and Packer and Henderson (1997), present weld effective length rules for designers derived from this research. McFadden and Packer (2014) and Tousignant and Packer (2015) have shown that the fillet weld "directional strength-increase factor" ($1.00+0.50\sin^{1.5}\theta$) in Section J2.4 of AISC 360 (AISC 2016), and its equivalent of ($1.00+0.50\sin^{1.5}\theta)M_w$ in Clause 13.13.2.2 of CSA S16 (CSA 2014), does not provide adequate structural reliability (or safety) when used in conjunction with the rules for weld effective lengths. AISC (2011) and CISC (2016) hence disallow the use of the directional strength-increase, or "sinθ factor", when these rules are used to design fillet welds in HSS-to-HSS connections.

Packer et al. (2016) subsequently performed a large number of laboratory tests on HSS-to-rigid end-plate connections to investigate the applicability of the sinθ factor to one-sided fillet welds to HSS, joined to a rigid end-plate. These experiments removed the influence of a flexible landing surface for the fillet weld, and hence removed the weld effective length phenomenon. It was shown that HSS-to-plate fillet welds still did not provide the adequate structural reliability if the sinθ factor was implemented.

The research herein is a numerical extension of this experimental work to determine (for HSS-to-rigid end-plate connections): (a) the extent to which fillet welds to RHS and circular hollow sections (CHS) are similar; (b) the effect of relative weld size (t_w/t_b), branch wall slenderness (B_b/t_b and D_b/t_b), and branch inclination angle (θ_i) on the weld strength; (c) the influence of performing a more advanced reliability analysis; and (d) if alternate expressions are more appropriate for estimating the strength of fillet welds to HSS.

EXPERIMENTATION ON FILLET-WELDED HSS-TO-RIGID END-PLATE CONNECTIONS

Packer et al. (2016) published the results of 33 total weld-critical HSS-to-rigid end-plate connections (see Fig. 1) tested at the University of Toronto between the mid-1980s and present. Thirteen of these tests were done by Frater (1986) on RHS-to-rigid end-plate connections, with fillet weld throat dimensions (t_w) ranging from 0.37 to 1.13 times the branch wall thickness (t_b). Frater (1986) found that, for connections with small welds ($t_w/t_b \leq 0.50$) and a branch inclination angle θ_i = 90°, rupture always occurred through the weld, around the entire branch perimeter (failure mode W). When welds were only slightly larger ($0.50 < t_w/t_b \leq 0.60$), rupture generally occurred within the weld, but was accompanied by rupture of the end-plate near the middle of the RHS branch member walls (failure mode WP). For connections with the largest welds tested ($0.81 \leq t_w/t_b \leq 1.13$), end-plate rupture governed failure, with only some weld rupture occurring at sharp angles around the RHS corners (failure mode P). When θ_i = 60°, Frater (1986) found that only the connection with the smallest weld size (t_w/t_b = 0.42, where t_w/t_b ranged from 0.42 to 1.00) ruptured through the weld, around the entire branch perimeter. The remaining three connections with θ_i = 60° ruptured in the end-plate, instead of the weld, along the heel of the connection.

Eight additional RHS-to-rigid end-plate connections, with θ_i = 90° and similar weld sizes to Frater (1986) ($0.46 \leq t_w/t_b \leq 0.76$), were tested by Oatway (2014). In all of these tests, rupture occurred through the weld, around the entire branch perimeter. In 12 tests on CHS-to-rigid end-plate connections conducted by the authors (Packer et al. 2016, Tousignant and Packer 2016), with $0.45 \leq t_w/t_b \leq 0.99$, the same failure mode was observed. Three tests on CHS-to-rigid end-plate connections were also performed at Tongji University, China (Wang et al. 2015); however, only one of them failed entirely by weld rupture. A second test failed by weld rupture combined with branch rupture in the heat-affected zone, and the third test did not reach the ultimate load.

HSS-TO-RIGID END-PLATE CONNECTION FINITE ELEMENT MODELS

In order to validate the numerical (finite element) modeling procedure used herein, 33 RHS- and CHS-to-rigid end-plate connection finite element models, replicating experimental tests, were developed using ANSYS (Swanson Analysis Systems 2011). These models covered the following geometric parameters: θ_i = 60° and 90°, $0.34 \leq t_w/t_b \leq 1.13$, CHS branches with $11.0 \leq D_b/t_b \leq 25.1$, and RHS branches with $13.4 \leq B_b/t_b \leq 16.3$.

General

Each FE connection was comprised of a single tension-loaded branch welded to an end plate, with fixed restraints applied to the nodes on the "underside" of the end-plate. When θ_i = 60°, one half of each FE connection could be modeled using symmetry boundary conditions parallel to the axis of the toe and heel of the connection (Figs. 2 and 3). When θ_i = 90°, an additional plane of symmetry, orthogonal to the first plane and through the center of the branch, allowed one quarter of each connection to be modeled. It was shown that these FE models provided identical load-displacement responses, and the same weld rupture loads, compared to FE models that included two concentric, tension-loaded, branches (welded to opposite sides of the end plate). Since two branches were used for the experimental tests in the manner described, it was necessary to demonstrate that the above models were equivalent, prior to evaluating them.

To ensure that load transfer was only through the fillet weld, a gap was used to separate the branch and the end-plate at their interface, as shown in Fig. 4. From preliminary analyses of the connections, the size of the gap was determined to have a significant effect on the non-linear response of the fillet weld. To take into account (and mitigate) this effect: (a) the size of the gap can be minimized (close to the Boolean tolerance of the FE program), and (b) the calculation of the weld throat area (A_w) can be done based on the portion of the fillet above the gap, as shown in Fig. 4. In applying (a) and (b), the load-displacement response and ultimate fracture strain of the FE models were found to closely agree with the experimental tests. Generally, however, when welds are much larger than the Boolean tolerance of the FE program, provision (b) is not necessary, since the size of the gap resulting from provision (a) will be small compared to weld leg dimensions (L_v and L_h).

Models were analyzed under static incremental displacements applied to the end of the branch, in the theoretical constant stress region identified by Mehrotra and Govil (1972) – a distance of $3B_b$ or $3D_b$ from the weld toe. It was therefore only necessary to model the portion of the branch within this distance.

Material Modeling

Multi-linear true stress-strain (σ_T - ε_T) curves were developed from corresponding engineering stress-strain (σ - ε) curves for the HSS, rigid end-plate, and weld metal, and used to describe the behavior of materials in the numerical models. Up to coupon necking, which corresponds to the ultimate engineering stress and strain (σ_u and ε_u, respectively), the σ - ε curve obtained from an average of three tensile coupon (TC) tests, in accordance with ASTM A370 (ASTM 2015), was converted to a σ_T - ε_T curve using the following relationships (Boresi and Schmidt 2003):

$$\sigma_T = \sigma(1+\varepsilon) \tag{1}$$

$$\varepsilon_T = ln(1+\varepsilon) \tag{2}$$

Eqs. (1) and (2) are not valid past the coupon necking point, since the stress distribution in the material is no longer uniaxial. Therefore, an iterative approach given by Ling (1996) was used to generate the remainder of the σ_T - ε_T curve. Ling's (1996) expression for the σ_T - ε_T curve in the necked region is given by Eq. (3):

$$\sigma_T = \sigma_T' \left[w(1+\varepsilon_T-\varepsilon_T') + (1-w)\left(\frac{\varepsilon_T^{\varepsilon_T'}}{\varepsilon_T'^{\,\varepsilon_T'}}\right)\right] \tag{3}$$

where σ_T' is the true stress at which necking starts, ε_T' is the true strain at which necking starts, and w is a weighting factor.

Ling's (1996) approach is based upon weighting an approximate lower- and upper-bound to the σ_T - ε_T curve past the coupon necking point. The lower bound (w = 0.0) represents a power law (Hollomon 1945), and the upper bound (w = 1.0) is linear (see Fig. 5).

The weighting constant, w, is determined by selecting a trial value of w to generate points on the σ_T - ε_T curve in the necked region (Fig. 5), running an incremental load-step analysis of a TC up to fracture and comparing the σ - ε curve from the model, which is generated from applied loads and nodal displacements, to experiments. The nodal displacements, and hence the FE strains, were calculated over a "virtual" 50-mm gage length from nodes on the exterior of the TC. This process is repeated until a value of *w* is found that results in acceptable agreement between the results.

For this work, TCs were modeled using average measured dimensions of the coupon widths and thicknesses (or diameters, for screw-type TCs), and nominal values of the grip dimensions, including the radius of the machined fillet and the length of the reduced section outside of the TC gage length (ASTM 2015). CHS TCs were modeled with curved geometries, as shown in Fig. 6, to replicate both the experimental tests, and the in-situ condition of the material. ANSYS SOLID45 8-noded brick elements, with non-linear material and geometric (large deformation) properties, were used.

The clip gage used to measure strain during the experimental tests was removed at $\varepsilon \cong 0.20$, to avoid damage; however, the elongation of the coupon and the load at rupture were measured and recorded. In the region of the σ - ε curve between first necking and the point where the clip gage was removed, where Ling's (1996) approach was used, the experimental and numerical results always showed good agreement (see Fig. 7). At the point of coupon rupture, agreement varied. In two previous FE studies (Voth and Packer 2012a; and Martinez-Saucedo et al. 2006), it was determined that rupture in large-scale HSS connections typically occurs at strains well below those present at the point of coupon rupture, due to boundary conditions and confinement in connections that are different from those in TCs. The gap between the HSS and the end plate also creates a crack-like feature at the root of the weld, which contributes to earlier rupture in the HSS connection relative to coupon specimens. Therefore, the variation in agreement between the numerical and experimental σ - ε curves at the point of coupon rupture was deemed of no consequence and, for the same reason, a fracture criterion was not calibrated for the TCs.

Model Sensitivity Study

To determine the element type and mesh arrangement best suited for modeling the HSS-to-rigid end-plate connections, a sensitivity study was performed. The sensitivity study investigated the relative load-displacement response of one RHS-to-rigid end-plate connection and one CHS-to-rigid end-plate connection, with different element types, mesh densities, numbers of HSS through-thickness elements, and elements along the weld face. The objective of the sensitivity study was twofold: (a) to determine the minimum mesh parameters necessary to obtain numerical convergence, and (b) to select a set of parameters for modeling the remainder of the RHS- and CHS-to-rigid end-plate connections, including those developed for the parametric study.

Two brick-type elements were examined for connection modeling: an 8-noded solid element with large deformation and strain capabilities and three translational degrees of freedom per node (SOLID45), and a 20-noded solid element capable of plasticity, creep, stress stiffening, large deflection, and large strain (SOLID95). In addition to element type, three different mesh layouts were assessed (fine, medium, and coarse, as shown in Fig. 8). Table 1 provides a summary of the different analyses performed for an RHS and CHS connection, showing what was varied. Regardless of the element type and mesh layout, all models produced similar results in terms of initial stiffness (the initial slope of the load-displacement curve), non-linear behavior response, and ultimate load (Fig. 9).

A medium mesh and SOLID45 elements (using reduced integration and hourglass control) were selected for the models based on the results of this study and previous HSS connection FE studies (Voth and Packer 2012a, 2012b) that also obtained good results with these parameters. Seven elements along the weld face and along the vertical weld leg, with six elements along the horizontal weld leg (see Fig. 4, shown previously), were found to be suitable for achieving good resolution of the weld response under applied loads. For the HSS, four through-thickness elements, biased towards the outside face of the branch in contact with the weld, were used to capture local stresses and bending effects due to eccentric loading. Three elements were used through the plate thickness; however, the number of plate through-thickness elements was found not to affect the results.

Model Fracture Criterion

Once the overall behavior of the FE models showed good agreement with the experimental tests, failure criteria were developed for the weld metal and the end-plate. These failure criteria were based upon a maximum equivalent strain (ε_{ef}), which was used to activate the "death feature" of an element in ANSYS. When the equivalent strain in an element reached ε_{ef}, the stiffness and the stress of that element were reduced to near zero (1 x 10^{-6}). The inactive element(s) thereafter shed load to surrounding elements (where the equivalent strain in the element, $\varepsilon_e < \varepsilon_{ef}$) and was permitted to freely deform. This element behavior is physically comparable to the initiation and propagation of a crack through the material.

The value of ε_{ef} to use in a model depends upon element boundary conditions, mesh arrangement and loading in the model, and has been found to vary from $\varepsilon_{ef} > 1.0$ (for unconfined elements in TCs) to $\varepsilon_{ef} < 0.20$. Martinez-Saucedo et al. (2006) used a value of $\varepsilon_{ef} = 0.60$ to model the fracture behavior of HSS in slotted end-plate connections, and Voth and Packer (2012a) used $\varepsilon_{ef} = 0.20$ to model similar behavior in CHS branch-plate connections.

For the current work, ε_{ef} for fracture in the weld ($\varepsilon_{ef,weld}$) and the end-plate ($\varepsilon_{ef,plate}$) was determined by comparison of the numerical and experimental load-displacement results. For the former, 10 experimental tests (four RHS-to-rigid end-plate tests and six CHS-to-rigid end-plate connection tests) were selected from the overall sample, and corresponding numerical models of each connection were analyzed. A value of $\varepsilon_{ef,weld}$ was hence determined, by trial and error, so that the FE displacement at failure matched the experimental displacement at failure in the full-scale experimental connection tests. Using displacements instead of loads provides a more robust means of determining $\varepsilon_{ef,weld}$, since fracture generally occurs on the plateau of the load-displacement curve. The mean values of $\varepsilon_{ef,weld}$ for the RHS- and CHS-to-rigid end-plate connection tests obtained were nearly equal (0.093 and 0.092, respectively), which hence gave credence to the use of an overall mean, 0.092, for the weld fracture criterion. The five experimental tests on RHS-to-rigid end-plate connections that exhibited end-plate rupture were selected from the overall sample to calibrate $\varepsilon_{ef,plate}$, producing a mean of 0.011.

The element "death feature" was thus programmed for elements in both the weld and the end-plate, as a loop within each load step, to determine the FE ultimate load ($P_{u,FE}$), the failure mode, and the sequence of failure (the location of first-cracking and subsequent crack propagation).

COMPARISON OF FE MODELS WITH EXPERIMENTAL ULTIMATE LOAD RESULTS

To validate the modeling techniques developed previously, the ultimate load and the failure mode predicted by the numerical models for each of the 33 HSS-to-rigid end-plate connections were compared to the experimental results. Table 2 presents key connection parameters, the experimental ultimate load ($P_{u,exp}$), the experimental failure mode, the FE-predicted ultimate load ($P_{u,FE}$) and the FE-predicted failure mode. The ratio of the actual-to-predicted ultimate load for each test ($P_{u,exp}/P_{u,FE}$) is also given. Over all 33 tests, the mean of the ratio of actual-to-predicted ultimate load (A/P) is 1.00 and has a coefficient of variation (COV) of 0.12. The correlations of A/P by researcher, and branch angle, are also shown in Table 2. The poorest correlation resulted for the RHS-to-rigid end-plate connection tests by Frater (1986), with θ_i = 60°. All but one of these specimens failed experimentally by end-plate rupture along the heel of the connection and weld rupture along the remaining three sides.

The numerical models provided good predictions for $P_{u,exp}$, and generally gave the correct failure mode. Only three out of the 33 models did not predict the correct failure mode (nos. 6, 8 and 14). From separate analyses, in which failure was constrained to either the end-plate or the weld, it was found that specimens nos. 6 and 8, which were predicted to fail at least partially in the plate, were within 3% of the load at which weld failure would have governed. Similarly, the end-plate rupture load for specimen no. 14 was only 5% higher than $P_{u,FE}$ (for weld failure) given in Table 2.

Frater's (1986) tests showed that it is possible for cracks that begin in the weld to propagate into the plate, or vice versa. Since the FE models were terminated once $P_{u,FE}$ was reached (to avoid problems that would later occur with convergence), it is not possible to determine if this phenomenon would have occurred in the numerical tests. However, to assess failure progression numerically from first cracking (the death of the first element) to ultimate load ($P_{u,FE}$), a list containing the numbers of "killed" elements was output from each load step in the analysis. It was found that the first weld elements to fail in the 90° RHS-to-rigid end-plate connections were generally close to the RHS corners, whereas the first plate elements to fail were near the middle of the RHS wall. These failure locations, and the progression of joint failure for specimen no. 13, which failed in the weld and the end-plate, are illustrated in Fig. 10.

Since the effect of landing surface flexibility was removed by welding to a rigid plate, the above behavior suggests that non-uniform stress distributions in RHS welded joints can still be caused by a difference in relative flexibility of the branch parallel to its surface, around its perimeter. It is also worth noting that element death typically occurred over several load steps in the RHS-to-rigid end-plate connection tests (i.e. a crack formed, and propagated), but occurred in a single load step in the CHS-to-rigid end-plate connection tests.

The first weld elements to fail in the 60° RHS-to-rigid end-plate FE models were located at the toe of the connection; and when end-plate failure did occur numerically the first end-plate elements to fail were also located at the toe [and not at the heel, as Frater (1986) observed]. Therefore, more experimental tests may be necessary to understand the conditions that lead to end-plate rupture in skewed HSS-to-rigid end-plate connections (θ_i < 90°).

COMPARISON OF FE MODELS WITH EXPERIMENTAL LOAD-DISPLACEMENT RESULTS

The numerical load-displacement curves were compared for 10 tests to the corresponding experimental load-displacement curves. Figs. 11 and 12 show these comparisons for the RHS- and CHS-to-rigid end-plate connections, respectively, wherein the numerical results are shown by solid lines and the experimental results are shown by dashed lines. For clarity, the experimental and FE load-displacement curves have been divided over two plots within each figure. Differences between these data are believed to be caused by fluctuations in the experimental weld dimensions around the branch perimeter, which were difficult to mitigate (by grinding), especially around RHS corners. For the connection numerical modeling, average values of t_w, L_v and L_h were used, and hence the effect of weld size variation is not included. Weld penetration has also been ignored. Despite this, the numerical and experimental ultimate loads, initial stiffnesses, and load-displacement responses, showed good agreement.

NUMERICAL PARAMETRIC STUDY OF HSS END-PLATE CONNECTIONS

A numerical parametric study was thus conducted in which 65 90° fillet-welded RHS- and CHS-to-rigid end-plate connection specimens with six values of t_w/t_b (ranging from 0.35 - 1.41), and six values of the branch wall slenderness (ranging from 9.1 - 50), were analyzed to determine the effect of key connection parameters on the fillet-weld strength. The effect of θ_i on the fillet-weld strength was thereafter addressed by conducting eight additional analyses of specimens with t_w/t_b = 0.50: two RHS-to-rigid end-plate specimens with B_b/t_b = 12.5 and 50, and θ_i = 60°; two RHS-to-rigid end-plate specimens with B_b/t_b = 12.5 and 50, and θ_i = 75°; two CHS-to-rigid end-plate specimens with D_b/t_b = 12.5 and 50, and θ_i = 60°; and two CHS-to-rigid end-plate specimens with B_b/t_b = 12.5 and 50, and θ_i = 75°. Then, these eight analyses were combined with four of the previous FE analyses on specimens with θ_i = 90° and t_w/t_b = 0.50 (two RHS-to-rigid end-plate specimens with B_b/t_b = 12.5 and 50, and two CHS-to-rigid end-plate specimens with D_b/t_b = 12.5 and 50) to investigate the change in weld strength with branch angle. The HSS width, or diameter, and end-plate thickness were kept constant for all joints (B_b = 200 mm, D_b = 168 mm, and t_p = 25 mm, respectively), and fillet welds were modeled with equal-sized legs. A 0.25 mm gap between the branch member and the end-plate was used to restrict load transfer to the weld. All models employed SOLID45 8-noded hexahedral elements and were permitted to fail either by weld or end-plate rupture, using the fracture criterion discussed previously.

The $\sigma_T - \varepsilon_T$ curves for each of the materials (cold-formed HSS, end-plate, and weld metal) (see Fig. 13) were directly developed from experimental TC tests, and used for all connections irrespective of geometry and branch type. The materials used had the following properties: yield stress of HSS (F_y) = 421 MPa, ultimate stress of HSS (F_u) = 501 MPa, yield stress of end-plate (F_{yp}) = 409 MPa, ultimate stress of end-plate (F_{up}) = 566 MPa, yield stress of weld metal (F_{yw}) = 501 MPa, and ultimate stress of weld metal (X_u) = 571 MPa. These values were chosen to provide a similar level of base metal and weld metal over-strength (the difference between the actual and minimum specified values used in design), to represent the standard assumption in connection design that matched electrodes are used. Outside and inside corner radii of the RHS (r_o and r_i) were taken as $2.0t_b$ and $1.0t_b$, respectively.

Early in the study, it was found that significant yielding of the branch occurred in CHS-to-rigid end-plate specimens with t_w/t_b-ratios exceeding 1.06. Thus, the range of t_w/t_b was reduced to $0.35 \leq t_w/t_b \leq 1.06$ for the CHS specimens. Tables 3 and 4 show the non-dimensional connection parameters for all models in the parametric study.

Results and Analysis

Weld rupture occurred in 22 out of 35 tests on 90° RHS-to-rigid end-plate connections, and 25 out of 30 tests on 90° CHS-to-rigid end-plate connections. In 21 and 20 of these tests, respectively, weld rupture occurred before branch yielding. End-plate rupture occurred before weld rupture and branch yielding in nine of the RHS-to-rigid end-plate connection tests, and two of the CHS-to-rigid end-plate connection tests. The non-dimensional average stress on the weld throat at failure ($P_{u,FE}/A_wX_u$), and the failure mode(s), were hence recorded (Tables 3 and 4). For the tests that failed by weld rupture, the factor $P_{u,FE}/A_wX_u$ relates the shear strength of the weld metal to the electrode ultimate strength. In general, $P_{u,FE}/A_wX_u$ decreased as the RHS or CHS branch became more slender, and as the weld became larger with respect to the branch thickness.

The FE RHS-to-rigid end-plate connections that failed by end-plate rupture, both before and after yielding of the branch, exhibited low values of B_b/t_b and high values of t_w/t_b, such that the ratio of t_w/t_b to B_b/t_b was always greater than 0.035 [Eq. (4)]. For the CHS-to-rigid end-plate connections that failed by end-plate rupture, the ratio of t_w/t_b to D_b/t_b was always greater than about twice that value, 0.072 [Eq. (5)].

For plate rupture of RHS-to-rigid end-plate connections:

$$\frac{\left(\frac{t_w}{t_b}\right)}{\left(\frac{B_b}{t_b}\right)} = \frac{t_w}{B_b} > 0.035 \tag{4}$$

For plate rupture of CHS-to-rigid end-plate connections:

$$\frac{\left(\frac{t_w}{t_b}\right)}{\left(\frac{D_b}{t_b}\right)} = \frac{t_w}{D_b} > 0.072 \tag{5}$$

When $t_w/B_b \leq 0.035$ or $t_w/D_b \leq 0.072$, weld rupture can be expected to govern. The use of non-dimensional parameters to study the behavior of HSS connections is a common practice which allows results to be generalized for all sizes of HSS; thus, Eqs. (4) and (5), and the remainder of the results, are believed to be valid for smaller or larger sizes of B_b or D_b than those selected in this study.

All of the end-plate ruptures in the numerical RHS-to-rigid end-plate connection models were observed at mid-wall of the RHS, a critical location validated by experimental tests (Frater 1986). Furthermore, the values of t_w/B_b for the experimental RHS-to-rigid end-plate connection specimens that failed by end-plate rupture satisfied Eq. (4). Since end-plate rupture did not occur in any of the experimental CHS-to-rigid end-plate connection specimens, more tests are necessary to validate Eq. (5) experimentally.

Effect of Relative Weld Size

Fig. 14 illustrates the effect of t_w/t_b on the weld strength, given by the ratios $P_{u,FE}/A_wX_u$ and $P_{u,exp}/A_wX_u$. For both RHS- and CHS-to-rigid end-plate connections, as t_w/t_b increased (for constant values of B_b/t_b and D_b/t_b), $P_{u,FE}/A_wX_u$ decreased. The magnitude of the effect of t_w/t_b on the weld strength was found to be similar for both the RHS- and CHS-to-rigid end-plate connections; however, fillet welds in CHS-to-rigid end-plate connections generally exhibited a higher average strength.

In general, as t_w/t_b increases, the eccentricity (equal to the distance from the middle of the branch wall to the centroid of the fillet weld) increases, and the moment transmitted about the longitudinal axis of the weld increases. This moment causes bending of the branch wall inward and tension near the weld root, which is well-known to be a situation that can lead to premature weld failure. This detrimental feature of "one-sided fillet welds" is inherent to all HSS fillet-welded joints. Fig. 15, from FE analysis, illustrates this effect for two fillet-welded RHS joints. In Fig. 15, the von Mises equivalent stress is overlaid atop the deformed RHS branch member and the weld at failure.

Effect of Branch Wall Slenderness

Fig. 16 illustrates the effect of B_b/t_b and D_b/t_b on $P_{u,FE}/A_wX_u$. As B_b/t_b and D_b/t_b increased (i.e. the branch became more slender), the strength of joints that failed by weld rupture also decreased slightly. This effect was more pronounced for RHS-to-rigid end-plate connections than CHS-to-rigid end-plate connections. At low values of B_b/t_b, the fillet-weld strength in the RHS-to-rigid end-plate connections approached a similar strength to that of a fillet weld in a CHS-to-rigid end-plate connection with low- to moderate values of D_b/t_b, thereby corroborating the presence of local stiffness effects in RHS branches.

Connections with slender branches and high values of t_w/t_b exhibited significant rotations of the branch wall adjacent to the weld inwards at failure, as shown previously in Fig. 15. When this rotation was small (i.e. branches were stocky, and t_w/t_b was small), $P_{u,FE}/A_wX_u$ was closer to the value predicted using the directional strength-increase factor, thus illustrating that fillet-welded RHS- and CHS-to-rigid end-plate connections merit special attention, since geometric parameters greatly influence the fillet weld strength.

Effect of Branch Inclination Angle

Fig. 17 illustrates $P_{u,FE}/A_wX_u$ as a function of θ_i for $\theta_i = 60°$, 75° and 90°, and two different values of the branch wall slenderness. Although the absolute strength of the weld increased due to the longer weld length as θ_i went from 90° to 60°, the effect on $P_{u,FE}/A_wX_u$ was negligible. The curves predicted using the sinθ factor in AISC 360 (2016) for the average loading angle of welds in RHS- and CHS-to-plate connections with various branch inclination angles are plotted in Fig. 17. Note that these equations neglect any provisions for deformation compatibly, but for $60° \leq \theta_i \leq 90°$ in an HSS joint this reduction is less than 4% using the M_w factor in CSA S16 (2014) with the average loading angle of the weld. While the directional strength-increase factor predicts a reduction in $P_{u,FE}/A_wX_u$ as θ_i decreases from 90° to 60°, Fig. 17 illustrates that this is not always the case. Therefore, the complex effect of θ_i on fillet weld strength may reasonably be ignored for weld joints to HSS, and the weld strength (per unit length) may be considered independent of the branch angle.

ALTERNATE MODEL FOR FILLET WELD STRENGTH IN HSS JOINTS

It can be seen from the previous comparisons that $P_{u,FE}/A_wX_u$ in HSS-to-rigid end-plate connections is non-constant, and that it is a function of both t_w/t_b and B_b/t_b (or D_b/t_b). Linear regression analyses were hence performed on the results of the numerical RHS- and CHS-to-rigid end-plate connections to develop alternate, yet still simple, equations for predicting the strength of fillet welds in such connections. These regressions were comprised only of the data from the FE tests that failed by weld rupture before branch yielding. Preliminary regressions, with $P_{u,FE}/A_wX_u$ as the dependant variable and t_w/t_b and B_b/t_b (or D_b/t_b) as the independent variables, yielded the following equations for the strength of fillet welds to HSS:

For RHS: $$\frac{P_{u,FE}}{A_wX_u} = 0.954 - 0.00193\left(\frac{B_b}{t_b}\right) - 0.210\left(\frac{t_w}{t_b}\right) \tag{6}$$

For CHS: $$\frac{P_{u,FE}}{A_wX_u} = 1.009 - 0.00137\left(\frac{D_b}{t_b}\right) - 0.197\left(\frac{t_w}{t_b}\right) \tag{7}$$

which provide R^2 values of 0.97 and 0.93, respectively, and mean A/P ratios and COVs of 1.00 and 0.02 (both are the same) when compared to the numerical results.

According to Eqs. (6) and (7), the change in fillet weld strength as t_w/t_b increases from 0.35 to 1.05 is considerable, whereas the change in fillet weld strength as B_b/t_b (or D_b/t_b) increases from nine to 50 is small. It is therefore possible to neglect the effect of branch wall slenderness and still produce a sufficiently accurate equation for the ultimate strength of fillet welds to HSS, P_u (= $P_{u,exp}$ or $P_{u,FE}$), as follows:

For RHS: $$\frac{P_u}{A_w X_u} = 0.924 - 0.262\left(\frac{t_w}{t_b}\right) \quad (8)$$

For CHS: $$\frac{P_u}{A_w X_u} = 0.984 - 0.226\left(\frac{t_w}{t_b}\right) \quad (9)$$

Eqs. (8) and (9) provide R^2 values of 0.83 and 0.77, mean A/P values of 1.02 and 1.00, and COVs of 0.04 and 0.03, respectively, when compared to the numerical results. The correlations of Eqs. (8) and (9) against the numerical and experimental results are shown as dashed lines in Fig. 14 (presented earlier). While these are simple equations for predicting the strength of fillet welds to HSS, they are not well-suited for design because they are quadratic with respect to t_w (since $A_w = t_w l_w$). By simplifying the constants in Eqs. (8) and (9), and substituting P_r/P_y (where P_r is the required weld strength, in units of force, and P_y is the yield load of the branch) for t_w/t_b, Eqs. (8) and (9) can be rewritten as:

For RHS: $$R_n = \left[0.90 - 0.25\left(P_r/P_y\right)\right]A_w X_u \quad (10)$$

For CHS: $$R_n = \left[1.00 - 0.25\left(P_r/P_y\right)\right]A_w X_u \quad (11)$$

where R_n is the nominal weld strength (in units of force).

In a worst-case scenario, the required weld strength P_r will equal the ultimate weld strength P_u, which becomes disproportionately larger as t_w increases. The branch yield load P_y is linearly related to t_b. By comparing the relationship between the plotted points and the diagonal lines on Figs. 14 and 18, it can be seen that substituting t_w/t_b with P_r/P_y still provides a good prediction of the weld rupture load. Importantly, it also allows a solution to be found for t_w using a linear equation.

Comparing Eqs. (10) and (11) to the numerical results yields mean A/P values of 1.03 (both are the same), and COVs of 0.04 and 0.05, respectively. Comparing the same equations to the weld-critical experimental results yields mean A/P values of 1.08 and 1.04, and COVs of 0.17 and 0.10, respectively.

The correlation of Eq. (10) against the numerical and experimental RHS results, and the correlation of Eq. (11) against the numerical and experimental CHS results, is shown in Fig. 18.

RELIABILITY ANALYSIS OF FE RESULTS FOR DESIGN CODES

The mean values $P_{u,FE}/A_wX_u$ for the weld-critical FE RHS- and CHS-to-rigid end-plate connections in Fig. 18 are 0.75 and 0.84, respectively. These values are in very good agreement with the value of 0.80 for transverse one-sided fillet weld experiments reported by Vreedenburgh (1954), on non-HSS specimens. Additionally, the value of 0.75 for RHS is in good agreement with the values of 0.78 for RHS reported by Packer et al. (2016) (and Table 2), and the value of 0.84 for CHS is in good agreement with the value of 0.81 for CHS reported by Packer et al. (2016) (and Table 2), for the weld-critical experimental tests on HSS-to-rigid end-plate specimens. For both RHS and CHS, the values (0.75 and 0.84) are less than 0.90 and 1.005 predicted by AISC 360 (AISC 2016) and CSA S16 (CSA 2014) for transverse fillet welds (using the sinθ factor with $\theta = 90°$).

If capacities of the connections that failed by end-plate rupture (indicated by unfilled markers in Fig. 18) are calculated according to the weld metal shear strength, using the provisions of AISC 360 (AISC 2016) or CSA S16 (CSA 2014) with the sinθ factor, the test-to-predicted ratios will always be less than unity, as indicated by the markers being below the respective horizontal lines (0.90 and 1.005). Both AISC 360 (AISC 2016) and CSA S16 (CSA 2014) without the sinθ factor are more conservative for the prediction of the joint strength for numerical tests that failed by end-plate rupture (relative to the 0.60 and 0.67 lines in Fig. 18), but still do not always result in test-to-predicted strength ratios greater than unity.

Reliability Analysis Methodology

The ultimate strengths of the connections in the numerical tests were compared to the capacities predicted by AISC 360 (AISC 2016), CSA S16 (CSA 2014) and Eurocode 1993-1-8 (CEN 2005), in the manner outlined by Packer et al. (2016).

Table 5 summarizes the mean actual-to-predicted weld strengths (for various code models) for the RHS- and CHS-to-rigid end-plate connection specimens considered separately and together, and looking at specimens that failed by weld rupture only, or all specimens that failed by weld rupture or end-plate rupture (without yielding occurring in the branch). By comparing the mean A/P ratios given here to those published in Packer et al. (2016) (summarized in the right-most column), it can be seen that the numerical tests provide additional validation for their conclusions. Still, a more comprehensive reliability analysis is performed herein to determine if a sufficient safety margin is achieved by North American fillet weld design provisions if fillet welds to RHS branches are considered as a separate case, in the reliability analysis, to those to CHS branches.

It is common practice to assess the level of safety (or structural reliability) of a design model using a statistical method in which the resistance factor, ϕ (or ϕ_w), is calculated, from a prescribed safety index, β, according to Eq. (12) (Fisher et al. 1978; Ravindra and Galambos 1978):

$$\phi = \phi_\beta \rho_R \exp(-\alpha_R \beta V_R) \tag{12}$$

where α_R is the coefficient of separation, taken as 0.55 (Ravindra and Galambos 1978); ρ_R is the bias coefficient for the resistance (the ratio of the mean-to-nominal connection capacity considering all variations in material properties, geometry, and the model), and V_R is the COV of this ratio. The formulation of these terms is shown below.

$$\rho_R = \rho_M \rho_G \rho_P \tag{13}$$

$$V_R = \sqrt{V_M^2 + V_G^2 + V_P^2} \tag{14}$$

where ρ_M = mean measured-to-nominal material strength ratio; ρ_G = mean measured-to-nominal connection geometric properties ratio; ρ_P = mean professional factor (measured-to-predicted connection strength, where the predicted connection strength is calculated using all measured experimental values); V_M = coefficient of variation (COV) of ρ_M; V_G = COV of ρ_G; and V_P = COV of ρ_P.

The variation of the material properties is represented by ρ_M, and its respective COV, V_M. These factors are associated with the expected variability in X_u. A comparison of the ρ_M-values from Lesik and Kennedy (1990), which represents the largest database of all-weld-metal tensile coupon test results ever compiled (number of samples, n = 672), Callele et al. (2009), and recent University of Toronto test programs (McFadden and Packer 2014; and work by the authors) are given in Table 6. It is clear from

Table 6 that there is a trend towards increasingly higher strength weld metal; however, due to the limited number of recent tests, the composite mean and COV from the three studies (1.12 and 0.122, respectively), which give more weight to the larger sample of Lesik and Kennedy (1990), are used herein.

The mean measured-to-nominal connection geometric properties ratio, ρ_G, and its respective COV, V_G, are associated with the expected variability in the weld throat area ($A_w = t_w l_w$). For fillet weld joints to RHS, a survey of the research by Frater and Packer (1992a, 1992b), Packer and Cassidy (1995), McFadden and Packer (2014), and Tousignant and Packer (2015) indicated that the average actual-to-nominal weld length (i.e. the perimeter of the RHS) is 0.99 with a COV of 0.5%. It is expected that similar results would be found from a survey of fillet weld joints to CHS. In the current experiments, welding was closely monitored (a maximum leg size was generally enforced) and welds were ground flat prior to testing, so the mean value and variations in actual-to-nominal weld throat size cannot be scientifically obtained. However, Callele et al. (2009) justified the use of $\rho_G = 1.03$ and $V_G = 0.10$, which are adopted herein.

The safety index, β, is directly related to the probability of failure. According to AISC 360 (AISC 2016), for the load and resistance factor design (LRFD) method, the implied (or target) safety index for connections is 4.0 (per Chapter B of the Commentary to AISC 360). For members, this value is 2.6. The larger β-value for connections reflects the fact that connections are expected to be stronger than the members they connect. For limit states design in Canada, these values are stated to be 3.0 and 4.5, respectively (per Annex B of CSA S16).

Due to the interdependence of the resistance factor and the load factor in the formulation of the LRFD and limit states design methods, the use of a safety index other than 3.0 [in Eq. (12)] requires that a modification factor (ϕ_β) be applied to the resistance. Fisher et al. (1978) gave a procedure for determining the value of ϕ_β to use for connections. More recently, Franchuk et al. (2002) applied this procedure to determine ϕ_β for β-values ranging from 1.5 to 5.0, and mean live-to-dead load ratios (L/D) ranging from 0.5 to 2.0. For L/D = 1.0, Franchuk et al. (2002) gave Eq. (15) for ϕ_β:

$$\phi_\beta = 0.0062\beta^2 - 0.131\beta + 1.338 \tag{15}$$

and reported a correlation coefficient (R^2 value) of 1.00, and a maximum difference between ϕ_β calculated using Eq. (15) and the procedure outlined by Fisher et al. (1978) of 2.0%.

Since the AISC 360 (AISC 2016) LRFD method is calibrated to the allowable stress design method at L/D = 3.0 (per Chapter B of the Specification Commentary), it is necessary to examine the error produced by Eq. (15) when L/D = 3.0 instead of 1.0. For this case, Moore et al. (2010) gave the following equation:

$$\phi_\beta = 0.0093\beta^2 - 0.1658\beta + 1.4135 \tag{16}$$

For β = 4.0 and L/D = 1.0, ϕ_β = 0.913 (if β = 4.5 instead, ϕ_β = 0.874). For β = 4.0 and L/D = 3.0, ϕ_β = 0.899 (if β = 4.5 instead, ϕ_β = 0.856). The variation in ϕ_β with respect to L/D is therefore small. Furthermore, as pointed out by Franchuk et al. (2002), the use of Eq. (15) provides a good estimate of ϕ_β across representative L/D ratios in structures (which typically range from about 0.5 to 3.0). Eq. (15) is also consistent with a recommendation made by Fisher et al. (1978) to use ϕ_β = 0.88 as the adjustment factor when β = 4.5. Therefore, for the calculation of ϕ_β herein, Eq. (15) is adopted.

Reliability Analysis Results

Reliability analyses, taking into account the mean values and variations in the material, geometric and professional factors discussed above, were performed for the following design procedures:

(a) AISC 360 (2016) and CSA S16 (2014) (with and without the sinθ factor);
(b) EN 1993-1-8 (CEN 2005) Directional Method and Simplified Method; and
(c) the alternate method given by Eqs. (10) and (11).

Because the product $0.67\phi_w = 0.60\phi$, where ϕ_w = 0.67 and ϕ = 0.75, predicted weld resistances – and, therefore, the resulting reliability index – are identical for AISC 360 (AISC 2016) and CSA S16 (CSA 2014), both with and without the sinθ factor. The following calculations of β are therefore presented only for AISC 360 (AISC 2016) with respect to (a) above.

Table 7 summarizes the key parameters of the reliability analysis, which required iteration to determine compatible values for ϕ_β and β. Alternatively, one can directly calculate the resistance factor (ϕ_w or ϕ) required to meet the target safety index. In Table 7, Eqs. (10) and (11) have been assessed using ϕ =

0.75 and 0.67, to determine their reliability when used with the resistance factors for weld metal in AISC 360 (AISC 2016) and CSA S16 (CSA 2014), respectively.

By examining the β-values in Table 7, it can be seen that the sinθ factor is still unsafe (provides β less than the target value) when applied to fillet welds in HSS-to-rigid end-plate connections, irrespective of whether the branch is an RHS or CHS member, and even when the typical weld metal over-strength, which provides a beneficial effect, is considered. By examining ρ_P and β, respectively, for Eqs. (10) and (11), it can be seen that they provide both accurate predictions of fillet weld ultimate strength, and an adequate level of reliability (safety) for use in North America.

WELD SIZE TO DEVELOP THE YIELD STRENGTH OF A 90° HSS BRANCH

Eqs. (10) and (11) can therefore be used to determine the weld size required to develop the yield strength of a connected RHS or CHS branch member – a highly-debated topic internationally, and among code committees. In order to solve for t_w as a function of the branch wall thickness (t_b) using Eqs. (10) and (11), it is necessary to assume – conservatively – that the branch cross-sectional area (A_b) is equal to the product of the branch perimeter (i.e. the weld length, l_w) and t_b. By setting the nominal weld strength R_n and the required weld strength P_r equal to P_y, it can be shown that for an RHS branch:

$$t_w = \frac{1}{0.65}\left(\frac{F_y}{X_u}\right) t_b \tag{17}$$

will develop the branch yield strength. Therefore, for a 350W RHS branch member (F_{yb} = 350 MPa) welded all around with matched electrodes (X_u = 490 MPa):

$$t_w = 1.10 t_b \tag{18}$$

Similarly, for CHS members:

$$t_w = \frac{1}{0.75}\left(\frac{F_y}{X_u}\right) t_b \tag{19}$$

$$t_w = 0.95 t_b \tag{20}$$

To achieve the necessary level of reliability in North America, the values of $1.10t_b$ and $0.95t_b$ should be multiplied by the ratio of the resistance factor for branch yielding to the resistance factor for the weld metal [i.e. 0.90/0.75 = 1.20 in AISC 360 (AISC 2016), and 0.90/0.67 =1.34 in CSA S16 (CSA 2014)].

A more reasonable estimate for skewed branches ($\theta_i \neq 90°$) can be obtained by taking into account the longer weld length due to the branch angle, for example, by dividing Eq. (20) for CHS branches by the factor K_a given by the American Welding Society (AWS 2015):

$$K_a = \frac{1 + 1/\sin\theta_i}{2} \tag{21}$$

SUMMARY AND CONCLUSIONS

Finite element models were developed for RHS-to-rigid end-plate and CHS-to-rigid end-plate fillet welded connections and these were validated against 33 laboratory experiments on such welded joints. A parametric study was then performed in which a total of 73 FE models of RHS- and CHS-to-rigid end-plate connections were tested to failure under axial tension loading. The parametric study investigated the effect of the ratio of the weld throat dimension to the branch wall thickness (t_w/t_b), the branch wall slenderness (D_b/t_b and B_b/t_b) and the branch inclination angle (θ_i) on the weld strength. It was found that:

1. As t_w/t_b increases, the average stress on the weld throat area at failure significantly decreases.
2. As D_b/t_b and B_b/t_b increase, the average stress on the weld throat area at failure slightly decreases.
3. The branch inclination angle θ_i has a negligible effect on the weld strength per unit throat area; however, the longer weld length that results from a reduction in branch angle increases the absolute strength of the weld.

Equations were then developed to estimate the strength of fillet welds in RHS- and CHS-to-rigid end-plate connections. When subjected to a reliability analysis with respect to the weld-critical numerical results, these equations were found to provide an adequate level of safety for use in North America. It is shown, using these equations, that a weld throat dimension equal to $1.10t_b$ (for an RHS branch) and $0.95t_b$ (for a CHS branch) will develop the yield strength of the connected branch member at 90° to a rigid plate, for 350 MPa (50 ksi) yield-strength HSS with matching electrode.

The design methods for fillet welds to HSS members given in AISC 360 (AISC 2016), CSA S16 (CSA 2014), and EN1993-1-8 (CEN 2005) were evaluated with respect to North American safety index requirements, looking at fillet welds in RHS- and CHS-to-rigid end-plate connections independently, and using a reliability analysis that included the mean values and variations in material, geometric, and professional factors. The directional strength-increase factor in AISC 360 (AISC 2016) and CSA S16 (CSA 2014) was found to provide inadequate levels of the safety index when used to design fillet welds to HSS.

For all HSS connections, including HSS-to-HSS connections where the effective length concept is used, and even HSS connections in which the welds are fully effective, it is therefore recommended that the provisions of AISC 360 (AISC 2016) and CSA S16 (CSA 2014) for the design of fillet welds be used without the directional strength-increase factor [i.e. taking $\theta = 0°$ in the term $(1.00 + 0.50\sin^{1.5}\theta)$], or that the alternate method, developed herein, be used with North American resistance factors.

ACKNOWLEDGMENT

Financial support for this project has been provided by the Natural Sciences and Engineering Research Council of Canada (NSERC).

REFERENCES

AISC (American Institute of Steel Construction). (2011). "AISC commentary on the specification for structural steel buildings." *Steel Construction Manual, 14th ed.*, Chicago, IL.

AISC (American Institute of Steel Construction). (2016). "Specification for structural steel buildings." *ANSI/AISC 360-16*, Chicago, IL.

ASTM (American Society for Testing and Materials). (2015). "Standard test methods and definitions for mechanical testing of steel products." *ASTM A370-15*, West Conshohocken, PA.

AWS (American Welding Society). (2015). "Structural welding code – Steel, 23rd ed." *ANSI/AWS D1.1/D1.1M:2015*, Miami, FL.

Boresi, A. P. and Schmidt, R.J. (2003). *Advanced mechanics of materials, 6th ed.*, John Wiley and Sons, Inc., New Jersey, USA.

Callele, L. J., Driver, R. G. and Grondin, G. Y. (2009). “Design and behavior of multi-orientation fillet weld connections.” *Eng. J. AISC*, 46(4), 257-272.

CSA (Canadian Standards Association). (2014). “Design of steel structures.” *CSA S16-14*, Toronto, Canada.

CEN (Comité Européen de Normalisation). (2005). “Eurocode 3: Design of steel structures – Part 1-8: Design of joints.” *EN 1993-1-8:2005*, Brussels, Belgium.

CISC (Canadian Institute of Steel Construction). (2016). “Handbook of steel construction, 11th ed.” Toronto, Canada.

Fisher, J. W., Galambos, T. V., Kulak, G. L. and Ravindra, M. K. (1978). “Load and resistance factor design criteria for connectors.” *J. Struct. Div. ASCE*, 104(9), 1427-1441.

Franchuk, C. R., Driver, R. G. and Grondin, G.Y. (2002) “Block shear failure of coped steel beams.” *Proc., Annual Conference, CSCE*, Montreal, Canada.

Frater, G.S. (1986). *Weldment design for hollow structural section joints*. M.A.Sc. thesis, University of Toronto, Toronto, Ontario, Canada.

Frater, G. S. and Packer, J. A. (1992a). “Weldment design for RHS truss connections. I: Applications.” *J. Struct. Eng. ASCE*, 118(10), 2784-2803.

Frater, G. S. and Packer, J. A. (1992b). “Weldment design for RHS truss connections. II: Experimentation.” *J. Struct. Eng. ASCE*, 118(10), 2804-2820.

Hollomon, J. H. (1945). “Tensile Deformation,” *Trans. AIME*, 162, 268-290.

ISO (International Organization for Standardization). (2013). “Static design procedure for welded hollow section joints – Recommendations.” *ISO 14346:2013 (E)*, Geneva, Switzerland.

Lesik, D. F. and Kennedy, D. J. (1990). “Ultimate strength of fillet welded connections loaded in plane.” *Can. J. Civ. Eng.*, 17(1), 55-67.

Ling, Y. (1996). “Uniaxial true stress-strain after necking,” *AMP Journal of Technology*, 5(1), 37-48.

Martinez-Saucedo, G., Packer, J. A. and Willibald, S. (2006). “Parametric finite element study of slotted end connections to circular hollow sections.” *Engineering Structures*, 28(14), 1956-1971.

McFadden, M. R. and Packer, J. A. (2014). “Effective weld properties for hollow structural section T-connections under branch in-plane bending” *Eng. J. AISC*, 51(4), 247-266.

Mehrotra, B. L., and Govil, A. K. (1972). “Shear lag analaysis of rectangular full-width tube connections.” *J. Struct. Div., ASCE*, 98(ST1), 287-305.

Moore, A.M., Rassati G.A. and Swanson J.A. (2010) “An experimental analysis of strength and ductility of high strength fasteners.” *Eng. J. AISC*, 47(3), 161-174

Oatway, P. (2014). *Fillet-welded end-plate connections to square and rectangular HSS*. M.Eng. thesis, University of Toronto, Toronto, Ontario, Canada.

Packer, J. A. and Cassidy, C. E. (1995). “Effective weld length for HSS T, Y, and X connections.” *J. Struct. Eng. ASCE*, 121(10), 1402-1408.

Packer, J. A. and Henderson, J. E. (1997). *Hollow structural section connections and trusses – A design guide. 2nd ed.* Toronto, Canada: Canadian Institute of Steel Construction.

Packer, J. A., Sun, M., and Tousignant, K. (2016). “Experimental evaluation of design procedures for fillet welds to hollow structural sections.” *J. Struct. Eng. ASCE*, 10.1061/(ASCE)ST.1943-541X.0001476, 0416007.

Ravindra, M. K. and Galambos, T. V. (1978). “Load and resistance factor design for steel.” *J. Struct. Div. ASCE*, 104(9), 1337-1353.

Swanson Analysis Systems (2011). *ANSYS ver. 14.0*, Houston, TX.

Tousignant, K. and Packer, J. A. (2015). “Weld effective lengths for rectangular HSS overlapped K-connections.” *Eng. J. AISC*, 52(4), 259-282.

Tousignant, K. and Packer, J. A. (2016). “Experimental Evaluation of the Directional Strength-Enhancement Factor for Fillet Welds to CHS.” *Proceedings of the 8th International Workshop on Connections in Steel Structures*, Boston, MA.

Voth, A. P. and Packer, J. A. (2012a). “Branch plate-to-circular hollow structural section connections. I: Experimental investigation and finite-element modeling.” *J. Struct. Eng. ASCE*, 10.1061/(ASCE)ST.1943-541X.0000505, 995-1006.

Voth, A. P. and Packer, J. A. (2012b). "Branch plate-to-circular hollow structural section connections. I: X-type parametric numerical study and design." *J. Struct. Eng. ASCE*, 10.1061/(ASCE)ST.1943-541X.0000545, 1007-1018.

Vreedenburgh, G. G. J. (1954). "New principles for the calculation of welded joints." *Weld J.*, 33(8), 743-751.

Wang, W., Gu, Q., Ma, X. and Wang, J. (2015). "Axial tensile behavior and strength of welds for CHS branches to SHS chord joints." *Journal of Constructional Steel Research*, 115, 303-315.

NOTATION

The following symbols are used in this paper:

A_b = cross-sectional area of HSS branch member

A_w = effective throat area of weld

B_b = width of RHS branch member

CHS = circular hollow section

COV = coefficient of variation

CSA = Canadian Standards Association

D_b = diameter of CHS branch member

FE = finite element

F_u = ultimate strength of HSS

F_{up} = ultimate strength of end-plate

F_y = yield stress of HSS

F_{yp} = yield stress of end-plate

F_{yw} = yield stress of weld metal

H_b = height of RHS branch member

HSS = hollow structural section

K_a = effective length factor

L_h = weld leg length measured along the plate

LRFD = load and resistance factor design

l_w = total weld length

L_v = weld leg length measured along the HSS branch

M_w = strength reduction factor to allow for the variation in deformation capacity of weld elements with different orientations

P = applied force

P_r = required weld strength using LRFD load combinations

P_u = ultimate load

$P_{u,exp}$ = experimental ultimate load

$P_{u,FE}$ = FE ultimate load

$P_{u,FE}^{*}$ = FE load at experimental weld rupture displacement

P_y = yield load of HSS branch

RHS = rectangular hollow section

r_i = inside corner radius of RHS

R_n = nominal strength

r_o = outside corner radius of RHS

t_b = wall thickness of HSS branch member

TC = tensile coupon

t_p = end-plate thickness

t_w = weld effective throat thickness

V_G = COV of mean ratio of the measured-to-nominal values for the theoretical throat area

V_M = COV of mean ratio of the measured-to-nominal electrode ultimate strength (X_u)

V_P = COV of mean test-to-predicted capacity ratio

V_R = COV of the bias coefficient for the resistance

w = weighting factor

X_u = ultimate strength of weld metal

α_R = coefficient of separation

β = safety (reliability) index

ε = engineering strain

ε_e = equivalent (von Mises) strain

ε_{ef} = equivalent strain at rupture for failure criterion

$\varepsilon_{ef,plate}$ = equivalent strain at rupture for plate failure criterion

$\varepsilon_{ef,weld}$ = equivalent strain at rupture for weld failure criterion

ε_T = true strain

ε_T' = true strain at which necking starts

ε_u = ultimate engineering strain

γ_{M2} = partial safety factor for the resistance of weld = 1.25 in EN1003-1-8 (CEN 2005)

ϕ = resistance factor for the weld metal = 0.75 in AISC 360 (AISC 2016)

ϕ_w = resistance factor for weld metal = 0.67 in CSA S16 (CSA 2014)

ϕ_β = adjustment factor for $\beta \neq 3.0$

ρ_G = mean ratio of the measured-to-nominal values for the theoretical throat area

ρ_M = mean ratio of the measured-to-nominal electrode ultimate strength (X_u)

ρ_P = mean test-to-predicted capacity ratio

ρ_R = bias coefficient for the resistance

σ = engineering stress

σ_T = true stress

σ_T' = true stress at which necking starts

σ_u = ultimate engineering stress

θ = angle of loading of the weld

θ_i = branch inclination angle

LIST OF FIGURE CAPTIONS

Fig. 1. HSS-to-rigid end-plate connection specimens (with RHS or CHS members)

Fig. 2. FE CHS-to-rigid end-plate connection with $\theta_i = 60°$

Fig. 3. FE RHS-to-rigid end-plate connection with $\theta_i = 60°$

Fig. 4. Effective fillet weld dimensions in numerical RHS- and CHS-to-rigid end-plate connections

Fig. 5. Post-necking generated σ_T - ε_T curve using the Ling (1996) procedure (for CHS 127.4 × 11.55 TC)

Fig. 6. FE CHS TC (a) geometry and meshing, and (b) comparison of deformed shape results at fracture

Fig. 7. Comparison of numerical and experimental σ - ε curves (for CHS 127.4 × 11.55 TC)

Fig. 8. One-quarter FE model for non-inclined ($\theta_i = 90°$) CHS branch showing mesh arrangements investigated in the sensitivity study

Fig. 9. Load-displacement curves for CHS Specimen No. 26 with fine, medium and coarse mesh, and four CHS thickness elements

Fig. 10. Progression of joint failure in RHS-to-rigid end-plate specimen no. 13

Fig. 11. Comparison of RHS end-plate connection load-deformation behavior

Fig. 12. Comparison of CHS end-plate connection load-deformation behavior

Fig. 13. Engineering stress-strain curves for the cold-formed HSS, end-plate, and weld metal used in the parametric study

Fig. 14. Effect of the ratio t_w/t_b on weld strength in 90° HSS-to-rigid end-plate connections: (a) for RHS branches; (b) for CHS branches

Fig. 15. Examples of branch rotation in fillet-weld joints to RHS

Fig. 16. Effect of the ratios B_b/t_b and D_b/t_b on weld strength in HSS-to-rigid end-plate connections: (a) for RHS branches; (b) for CHS branches

Fig. 17. Effect of θ_i on weld strength in HSS-to-rigid end-plate connections

Fig. 18. Evaluation of design equations against all 90° (numerical and experimental) HSS-to-rigid end-plate connection test results: (a) for RHS branches; (b) for CHS branches

Table 1. FE mesh sensitivity study results

Specimen No. (Type)	Element Type	No. of elements	No. of nodes	HSS thickness elements	Plate thickness elements	Weld face elements	Mesh type	$P_{u,exp}$	$P_{u,\ FE*}$	$P_{u,exp}/P_{u,FE}^{*}$
2 (RHS)	SOLID45	15375	20554	3	3	7	Med.	1166	1208	0.97
	SOLID45	**18225**	**23512**	**4**		**7**	**Med.**		**1235**	**0.94**
	SOLID45	21075	26470	5		**7**	Med.		1240	0.94
	SOLID45	34340	43678	4		9	Fine		1232	0.95
	SOLID45	9747	12832	4		5	Coarse		1240	0.94
	SOLID95	9747	48140	4		5	Coarse		1268	0.92
26 (CHS)	SOLID45	11385	15470	3	3	7	Med.	841	828	1.02
	SOLID45	**13035**	**17206**	**4**		**7**	**Med.**		**832**	**1.01**
	SOLID45	14685	18942	5		7	Med.		833	1.01
	SOLID45	23160	30095	4		9	Fine.		832	1.01
	SOLID45	5680	7708	4		5	Coarse		838	1.00
	SOLID95	5680	28704	4		5	Coarse		842	1.00

Note 1: Specimen Nos. correspond to those given in Table 2.
Note 2: $P_{u,exp}$ = experimental ultimate load at weld rupture; $P_{u,FE}^{*}$ = FE load at experimental weld rupture displacement.

Table 2. Comparison of experimental and FE results for HSS-to-rigid end-plate connections

	Branch Type	Specimen No.	θ_i	$B_b \times H_b \times t_b$ (mm× mm× mm) or $D_b \times t_b$ (mm× mm)	A_b (mm^2)	B_b/t_b or D_b/t_b	t_w/t_b	$P_{u,exp}$ (kN)	Exp. Fail. Mode	$P_{u,FE}$ (kN)	FE Fail. Mode	$P_{u,exp}/P_{u,FE}$	mean (A/P)	COV
Oatway (2014)	RHS	1	90°	127.0 × 127.0 × 7.78 (r_0 = 15.88 mm) (r_i = 8.98 mm)	3563	16.3	0.46	831	W	841	W	0.99	1.04	0.10
		2					0.76	1166	W	1252	W	0.93		
		3					0.68	1235	W	1147	W	1.08		
		4					0.72	1311	W	1358	W	0.97		
	RHS	5	90°	177.8 × 177.8 × 12.53 (r_0 = 35.0 mm) (r_i = 23.4 mm)	7702	14.2	0.51	2433	W	2006	W	1.21		
		6					0.69	2574	W	2525	P	1.02		
		7					0.56	2525	W	2222	W	1.14		
		8					0.59	2302	W	2460	WP	0.94		
Frater [a] (1986)	RHS	9	90°	127.6 × 127.6 × 9.54 (r_0 = 19.08 mm) (r_i = 9.54 mm)	4271	13.4	0.44	1020	W	953	W	1.07	1.04	0.10
		10					0.37	960	W	805	W	1.19		
		11					0.34	840	W	733	W	1.15		
		12					0.50	1140	W	1116	W	1.02		
		13					0.60	1200	WP	1357	WP	0.88		
		14					0.57	1207	WP	1303	W	0.93		
		15					0.81	1494	P	1444	P	1.03		
		16					0.98	1578	P	1567	P	1.01		
		17					1.13	1788	P	1662	P	1.08		
	RHS	18	60°	127.6 × 127.6 × 9.54 (r_0 = 19.08 mm) (r_i = 9.54 mm)	4271	13.4	0.66	1131	WP	1531	W	0.74	0.83	0.14
		19					0.42	982	W	975	W	1.01		
		20					0.57	1270	WP	1590	WP	0.80		
		21					1.00	1534	WP	1905	WP	0.81		
Others	CHS	22	90°	167.9 × 6.70	3393	25.1	0.72	1261	W	1210	W	1.04	1.00	0.09
		23					0.99	1279	W	1523	W	0.84		
		24		127.4 × 11.55	4204	11.0	0.59	1459	W	1337	W	1.09		
		25					0.69	1597	W	1530	W	1.04		
		26		101.0 × 7.34	2160	13.8	0.87	841	W	860	W	0.98		
		27					0.84	864	W	877	W	0.99		
	CHS	28	60°	167.9 × 6.70	3393	25.1	0.79	1450	W	1207	W	1.20	1.02	0.12
		29					0.86	1331	W	1324	W	1.01		
		30		127.4 × 11.55	4204	11.0	0.45	1109	W	1278	W	0.87		
		31					0.59	1479	W	1601	W	0.92		
		32		101.0 × 7.34	2160	13.8	0.73	776	W	763	W	1.02		
		33					0.68	803	W	743	W	1.08		

Note: W = weld failure; WP = mixed failure mode of weld failure and partial plate failure; P = end-plate rupture along at least one weldment.

[a] r_i and r_o are taken as 1.0t_b and 2.0t_b, respectively, for all RHS used by Frater (1986).

Table 3. Parametric study results for RHS-to-rigid end-plate connections

B_b = 200 mm t_b (mm)	B_b/t_b	t_w/t_b					
		0.35	0.50	0.71	0.90	1.06	1.41
4.00	50	0.80 (W)	0.76 (W)	0.72 (W)	0.65 (W)	0.65 (W)	0.59 (W) *
5.00	40	0.80 (W)	0.77 (W)	0.73 (W)	0.69 (W)	0.67 (W)	**0.59 (P)** *
6.67	30	0.82 (W)	0.77 (W)	0.74 (W)	0.70 (W)	**0.67 (P)**	**0.56 (P)** *
10.00	20	0.84 (W)	0.80 (W)	0.76 (W)	**0.71 (P)**	**0.64 (P)**	**0.54 (P)** *
16.00	12.5	0.87 (W)	0.83 (W)	**0.72 (P)**	**0.63 (P)**	**0.56 (P)**	**0.49 (P)** *
22.00	9.1	0.88 (W)	0.84 (W)	**0.64 (P)**	**0.57 (P)**	**0.53 (P)**	- *

* Connections noted thus experienced branch yielding.

Note: W = rupture through the weld, around the entire branch perimeter; P = rupture only in the end-plate.

Table 4. Parametric study results for CHS-to-rigid end-plate connections

D_b = 168 mm t_b (mm)	D_b/t_b	t_w/t_b					
		0.35	0.50	0.71	0.90	1.06	1.41
3.36	50	0.85 (W)	0.87 (W)	0.81 (W)	0.76 (W)	0.73 (W) *	- *
4.20	40	0.89 (W)	0.86 (W)	0.82 (W)	0.76 (W)	0.73 (W) *	- *
5.59	30	0.88 (W)	0.88 (W)	0.82 (W)	0.78 (W)	0.74 (W) *	- *
8.40	20	0.90 (W)	0.88 (W)	0.85 (W)	0.80 (W) *	0.76 (W) *	- *
13.44	12.5	0.93 (W)	0.89 (W)	0.87 (W)	**0.79 (P)** *	**0.71 (P)** *	- *
18.48	9.1	0.92 (W)	0.90 (W)	**0.83 (P)**	**0.71 (P)**	**0.65 (P)** *	- *

* Connections noted thus experienced branch yielding.

Note: W = rupture through the weld, around the entire branch perimeter; P = rupture only in the end-plate.

Table 5. Mean FE-to-predicted (A/P) ratios and COVs (in parentheses) for code predictions of fillet weld nominal strength by AISC 360, CSA S16, and EN1993-1-8

	Weld Failure or Plate Failure			Weld Failure Only			Packer et al. (2016)
Branch Type	CHS	RHS	ALL	CHS	RHS	ALL	ALL
n	22	30	52	20	21	41	33
AISC 360-16 0.60	1.41 (0.07)	1.21 (0.13)	1.29 (0.13)	1.43 (0.06)	1.27 (0.09)	1.35 (0.09)	1.37 (0.27)
AISC 360-16 $0.60(1.00+0.50\sin^{1.5}\theta)$	0.94 (0.07)	0.80 (0.13)	0.86 (0.13)	0.95 (0.06)	0.85 (0.09)	0.90 (0.09)	0.93 (0.27)
CSA S16-14 0.67	1.27 (0.07)	1.08 (0.13)	1.16 (0.13)	1.28 (0.06)	1.14 (0.09)	1.21 (0.09)	1.23 (0.27)
CSA S16-14 $0.67(1.00+0.50\sin^{1.5}\theta)M_w$	0.84 (0.07)	0.72 (0.13)	0.77 (0.13)	0.85 (0.06)	0.76 (0.09)	0.81 (0.09)	0.83 (0.28)
EN1993-1-8:2005 Directional Method	1.23 (0.07)	1.05 (0.13)	1.13 (0.13)	1.24 (0.06)	1.11 (0.09)	1.17 (0.09)	-
EN1993-1-8:2005 Simplified Method	1.51 (0.07)	1.29 (0.13)	1.38 (0.13)	1.52 (0.06)	1.36 (0.09)	1.44 (0.09)	-

Table 6. Mean values and variations in actual-to-nominal ultimate strength of typical weld metal (X_u)

Study	n		ρ_M		V_M	
Lesik & Kennedy (1990)	672	707	1.12	1.12	0.077	0.122
Callele et al. (2009)	32		1.15		0.080	
Recent University of Toronto Test Programs[a]	3		1.22		0.042	

[a] nominal electrode strength is assumed to be 490 MPa for all electrodes tested.

Table 7. Reliability analysis parameters with respect to numerical results from weld-critical tests

	AISC 360-16 0.60		AISC 360-16 $0.60\times(1.00+0.50\sin^{1.5}\theta)$		EN1993-1-8: 2005 Directional Method		EN1993-1-8: 2005 Simplified Method		Eqs. (10) and (11)			
ϕ	0.75		0.75		$1/\gamma_{M2} = 0.80$		$1/\gamma_{M2} = 0.80$		0.75		0.67	
Branch Type	CHS	RHS	CHS	RHS	CHS	RHS	CHS	RHS	CHS	RHS	CHS	RHS
n	20	21	20	21	20	21	20	21	20	21	20	21
ρ_P	1.43	1.27	0.95	0.85	1.24	1.11	1.52	1.36	1.03	1.03	1.03	1.03
V_P	0.06	0.09	0.06	0.09	0.06	0.09	0.06	0.09	0.04	0.05	0.04	0.05
ρ_G	1.03											
V_G	0.10											
ρ_M	1.12											
V_M	0.12											
ρ_R	1.65	1.47	1.10	0.98	1.43	1.28	1.75	1.57	1.19	1.19	1.19	1.19
V_R	0.17	0.18	0.17	0.18	0.17	0.18	0.17	0.18	0.16	0.16	0.16	0.16
ϕ_β	0.78	0.84	0.95	1.02	0.86	0.92	0.79	0.84	0.91	0.91	0.86	0.86
β	5.87[a]	4.99[a]	3.56[b]	2.90[b]	4.68	3.90	5.97	5.03	4.12	4.06	4.76	4.68

[a] β identical to CSA S16 (2014) method without the $\sin\theta$ factor.
[b] β identical to CSA S16 (2014) method with the $\sin\theta$ factor.

Figure1

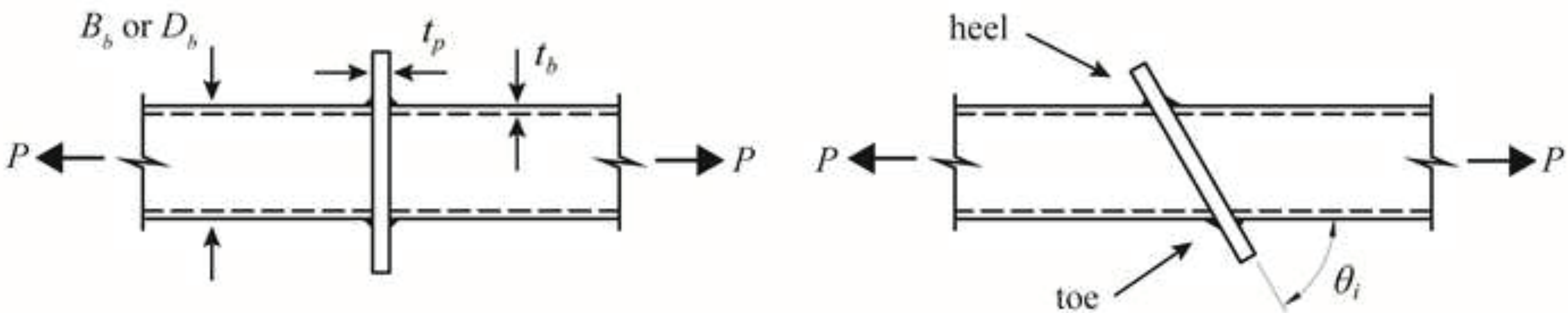

Figure2

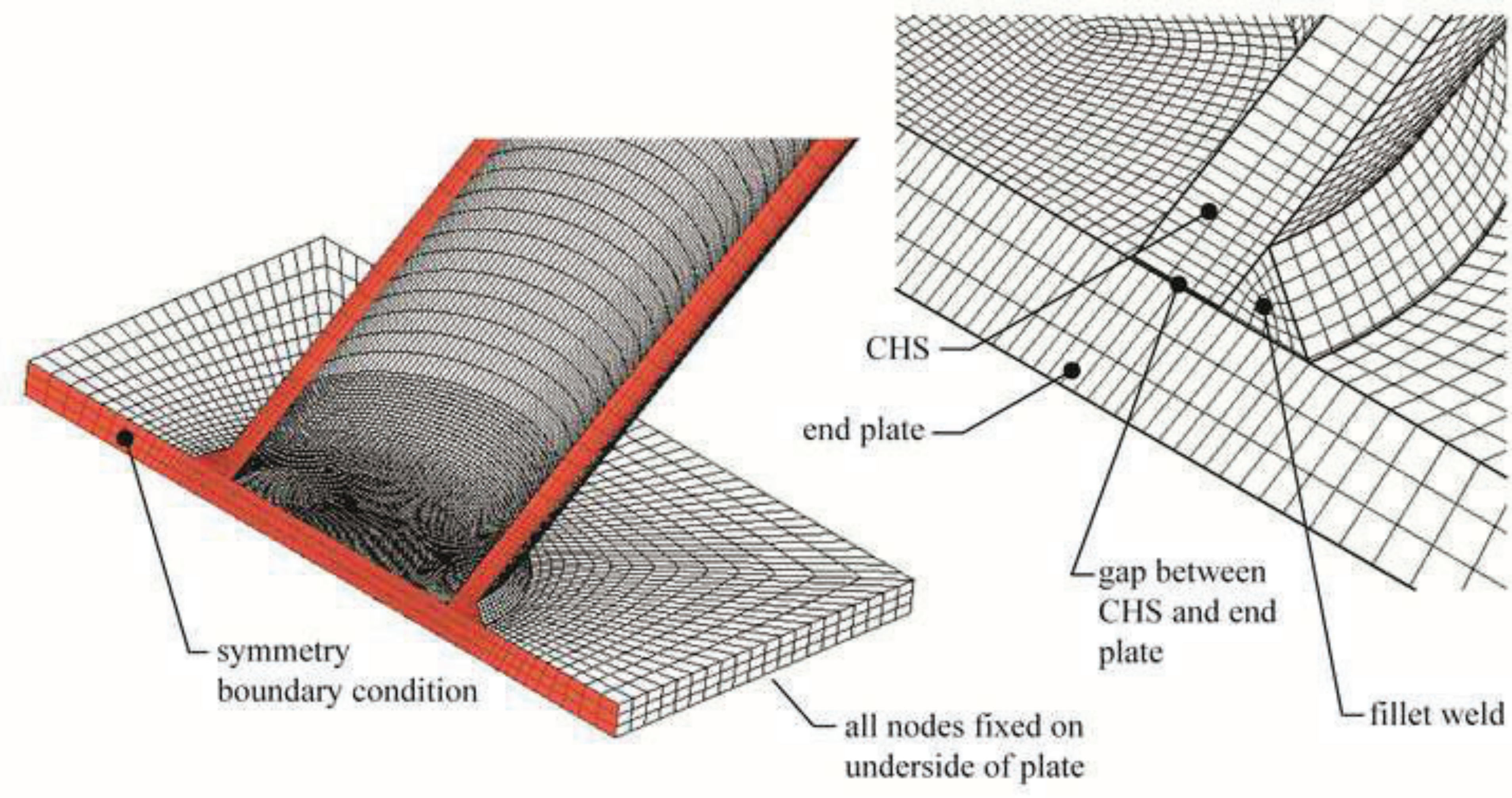
symmetry
boundary condition
all nodes fixed on
underside of plate
CHS
end plate
gap between
CHS and end
plate
fillet weld

Figure3

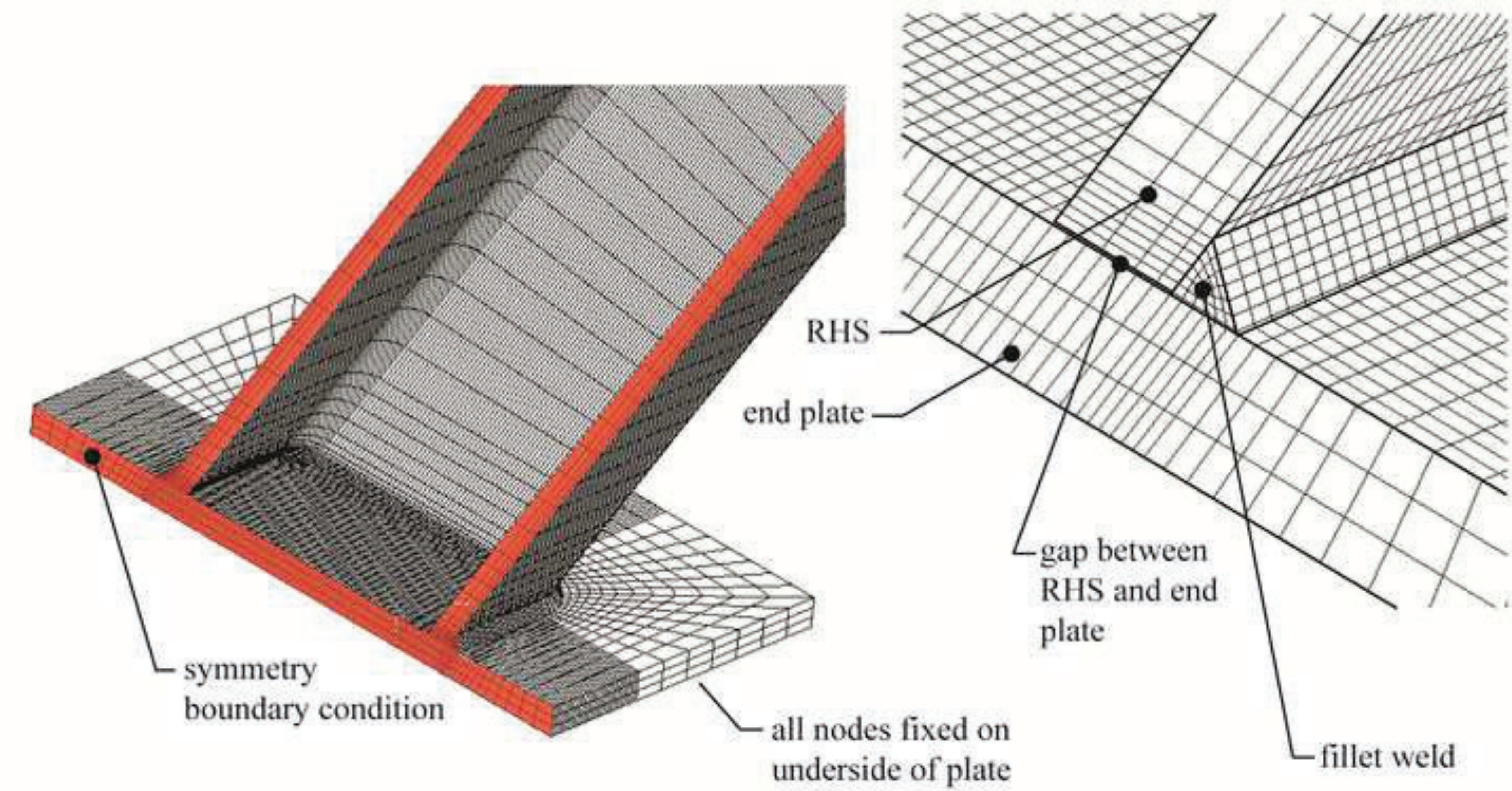
symmetry
boundary condition
all nodes fixed on
underside of plate
RHS
end plate
gap between
RHS and end
plate
fillet weld

Figure4

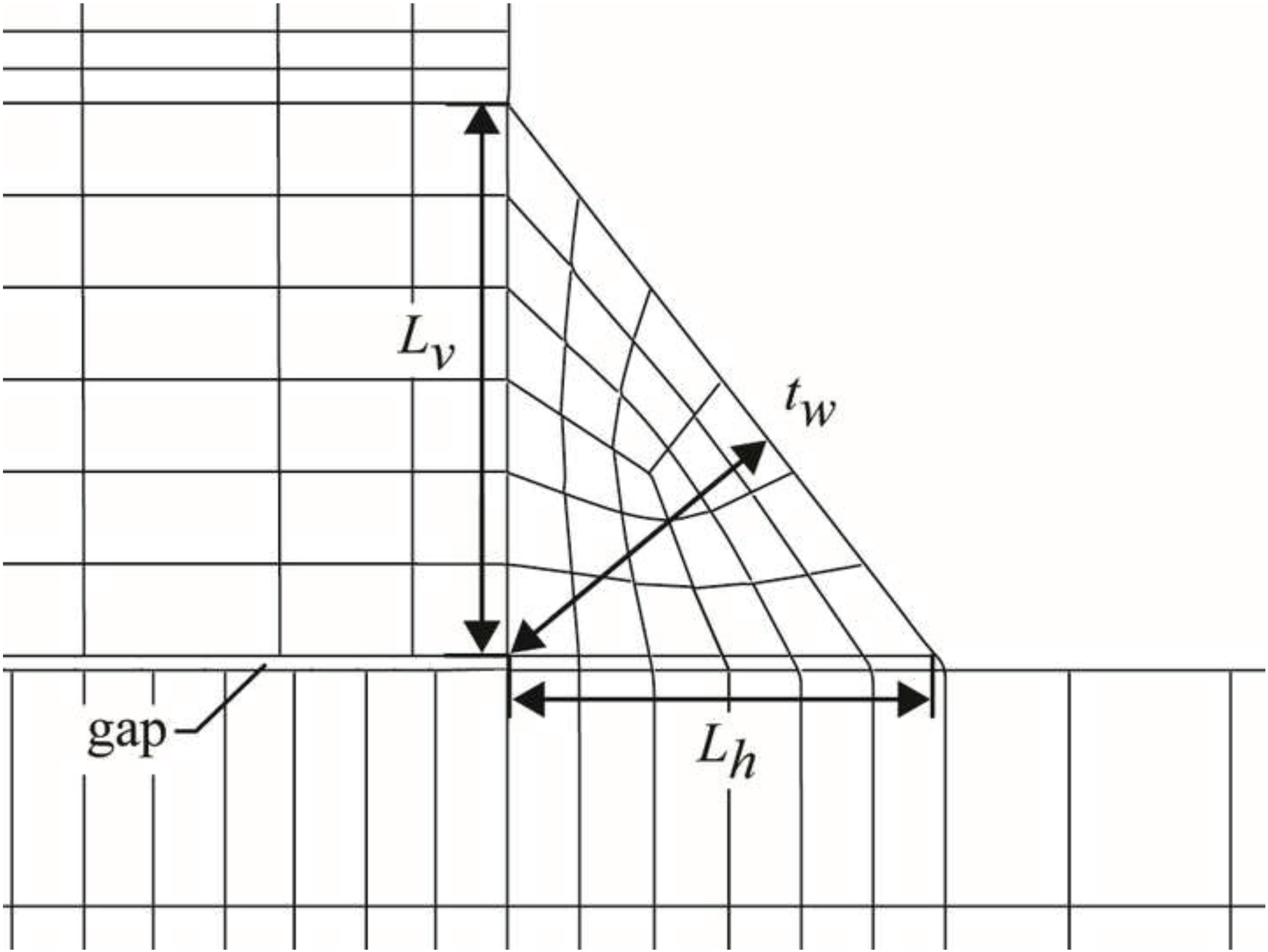

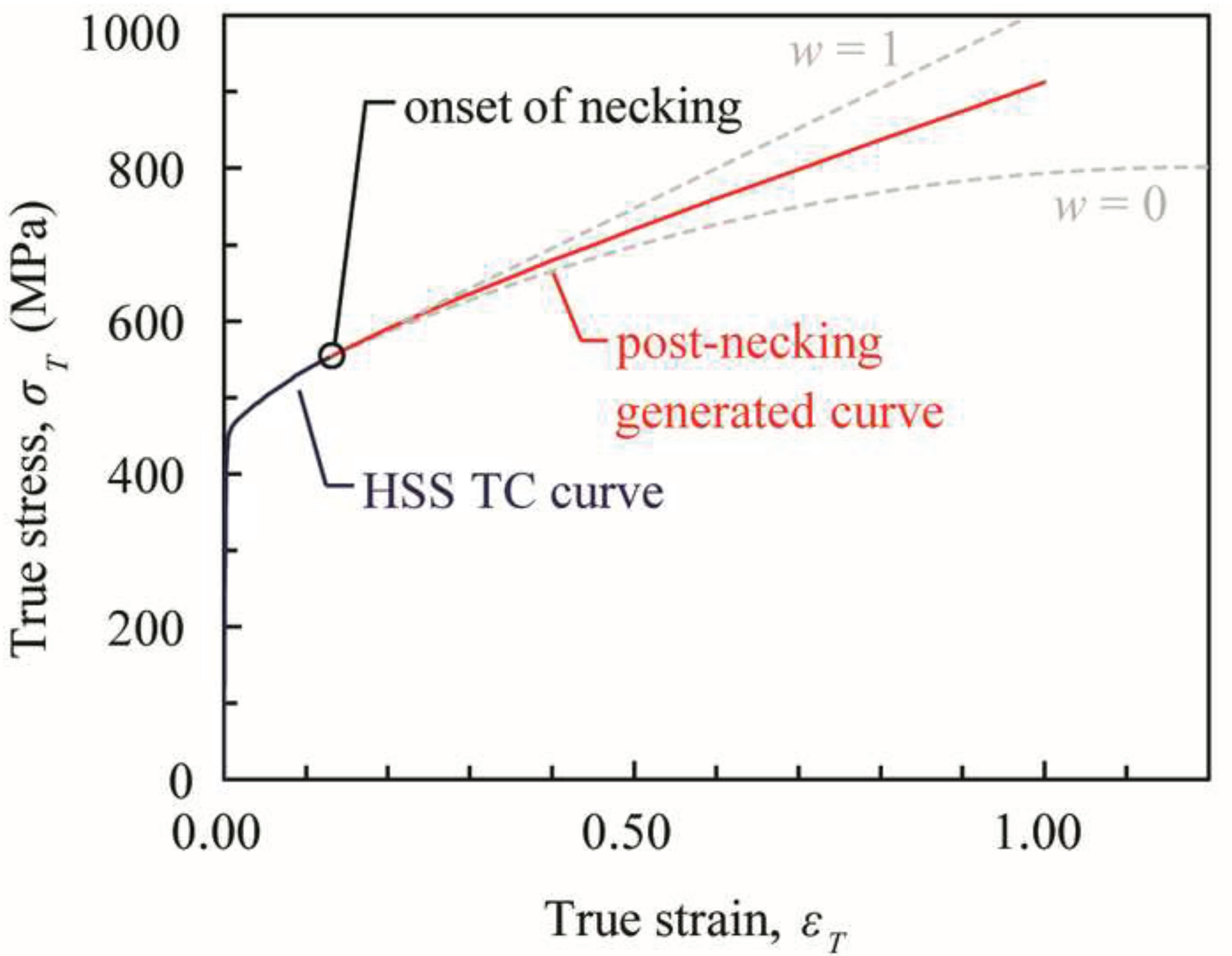
True stress, σ T (MPa)
1000
800
600
400
200
0
0.00
0.50
1.00
True strain, ε T
w = 1
w = 0
onset of necking
post-necking
generated curve
HSS TC curve

Figure6

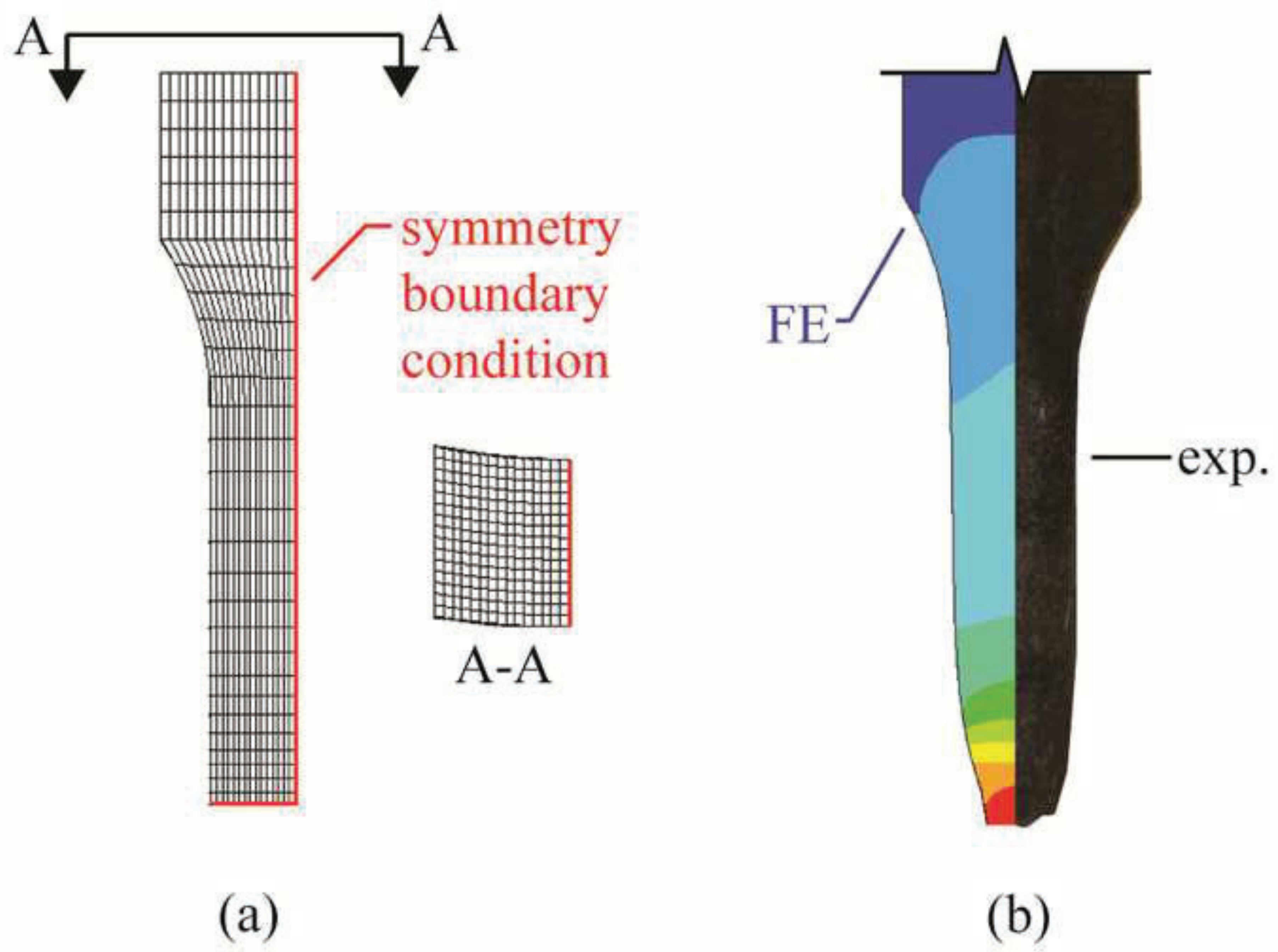

Figure7

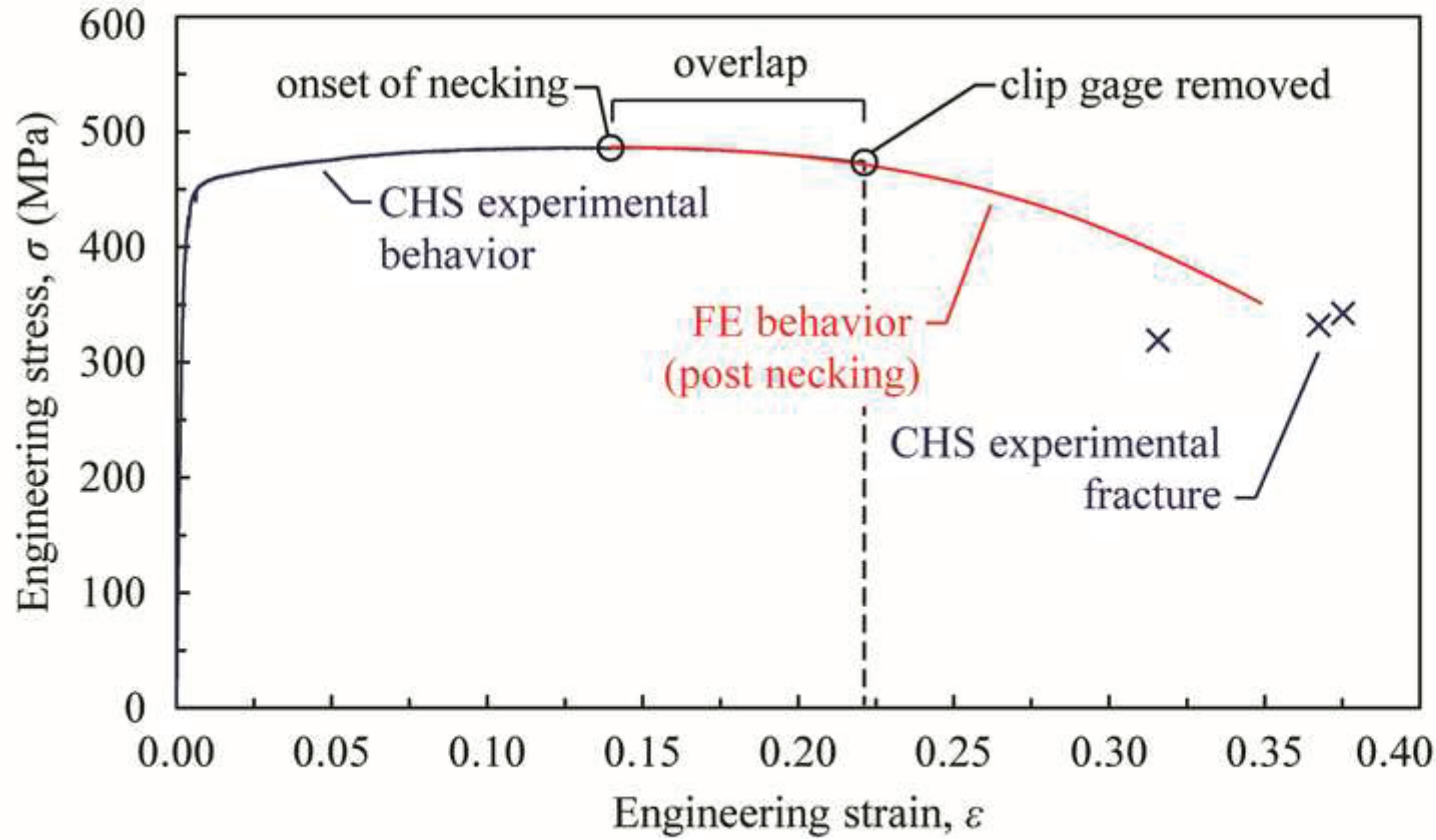
600
500
400
300
200
100
0
Engineering stress, σ (MPa)
0.00
0.05
0.10
0.15
0.20
0.25
0.30
0.35
0.40
Engineering strain, ε
onset of necking
overlap
clip gage removed
CHS experimental
behavior
FE behavior
(post necking)
CHS experimental
fracture

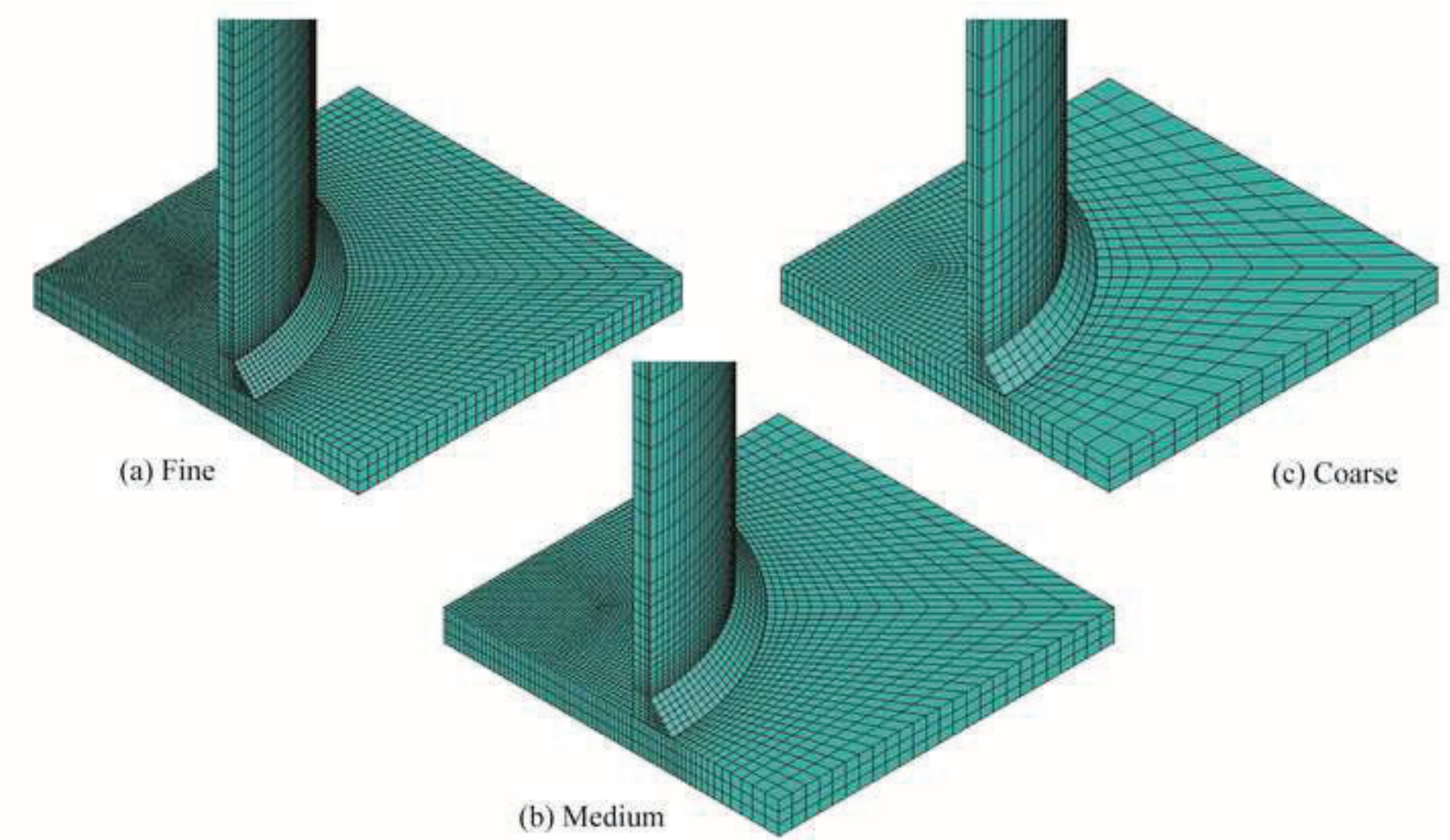
(a) Fine
(b) Medium
(c) Coarse

Figure9

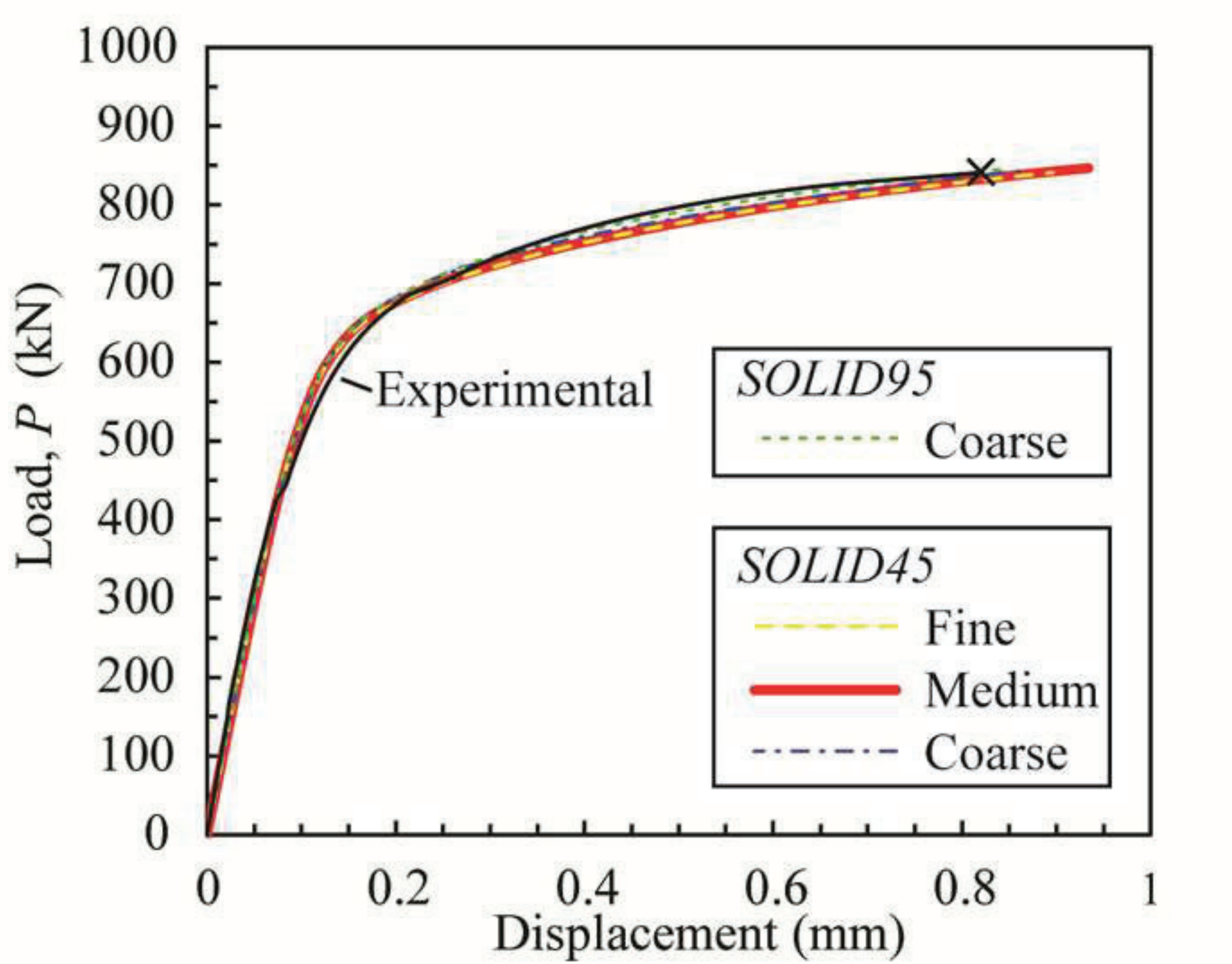

Load, P (kN)
1000
900
800
700
600
500
400
300
200
100
0
0
0.2
0.4
0.6
0.8
1
Displacement (mm)
Experimental
SOLID95
Coarse
SOLID45
Fine
Medium
Coarse

Figure10

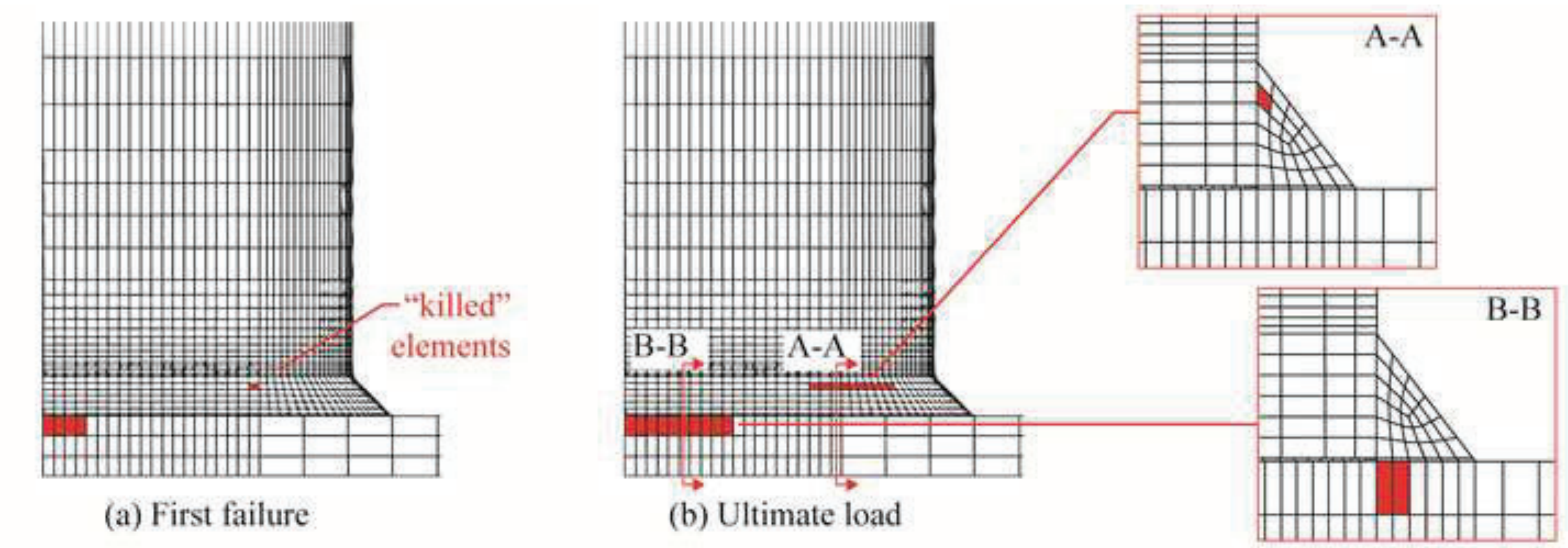

Figure11a

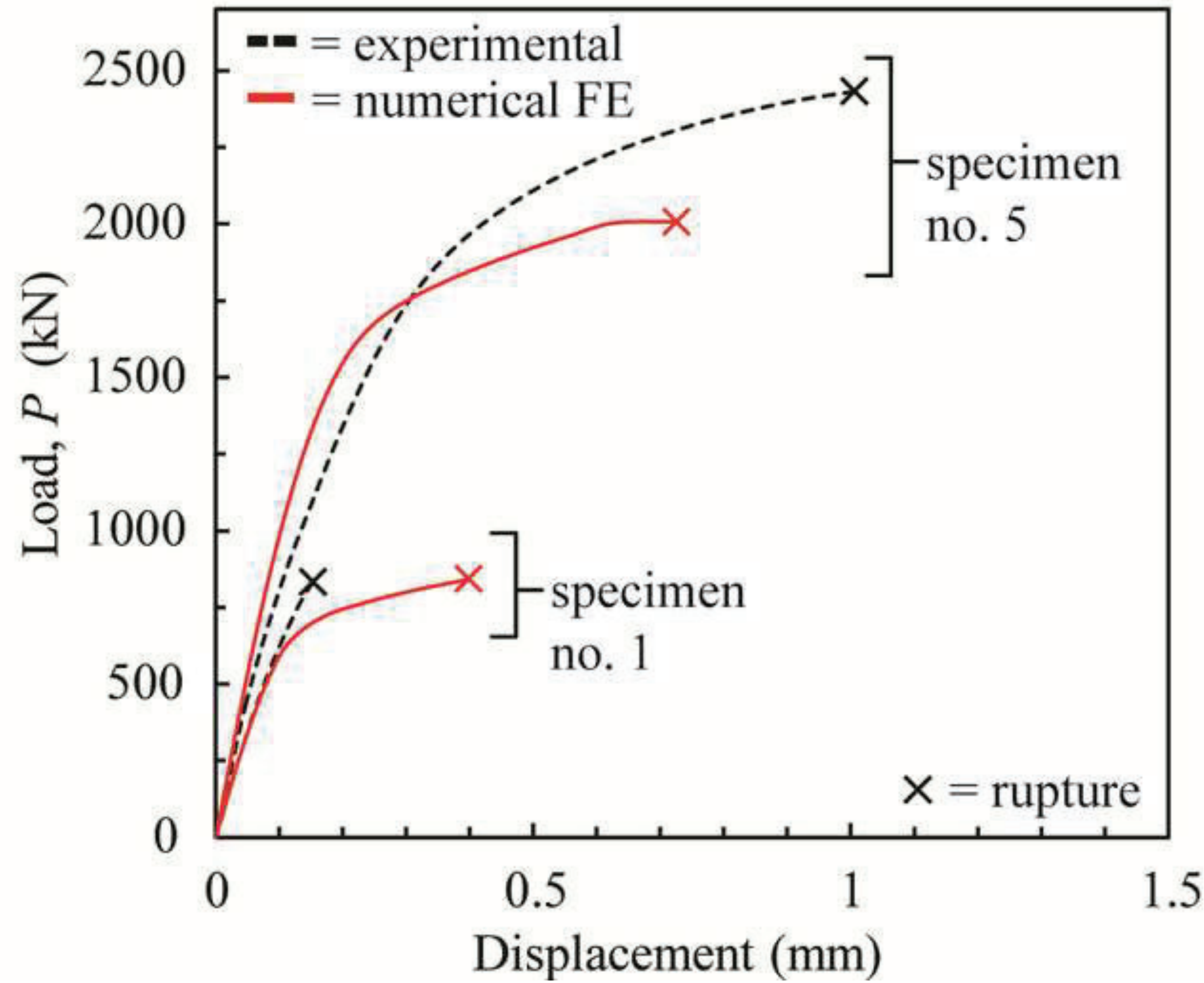
= experimental
= numerical FE
specimen
no. 5
specimen
no. 1
× = rupture
Load, P (kN)
2500
2000
1500
1000
500
0
0
0.5
1
1.5
Displacement (mm)

Figure11b

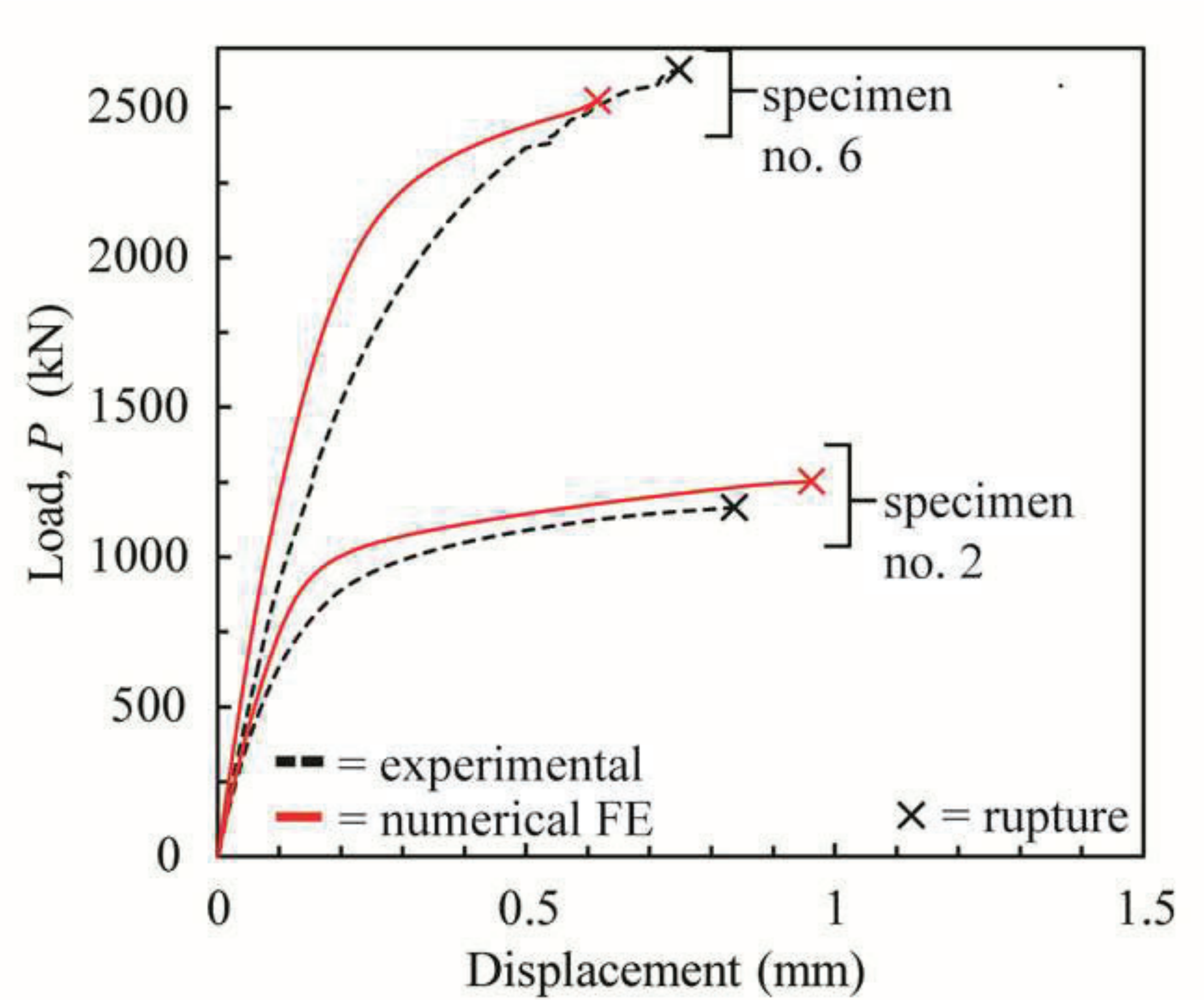
2500
2000
1500
1000
500
0
Load, P (kN)
0
0.5
1
1.5
Displacement (mm)
specimen
no. 6
specimen
no. 2
= experimental
= numerical FE
× = rupture

Figure12a

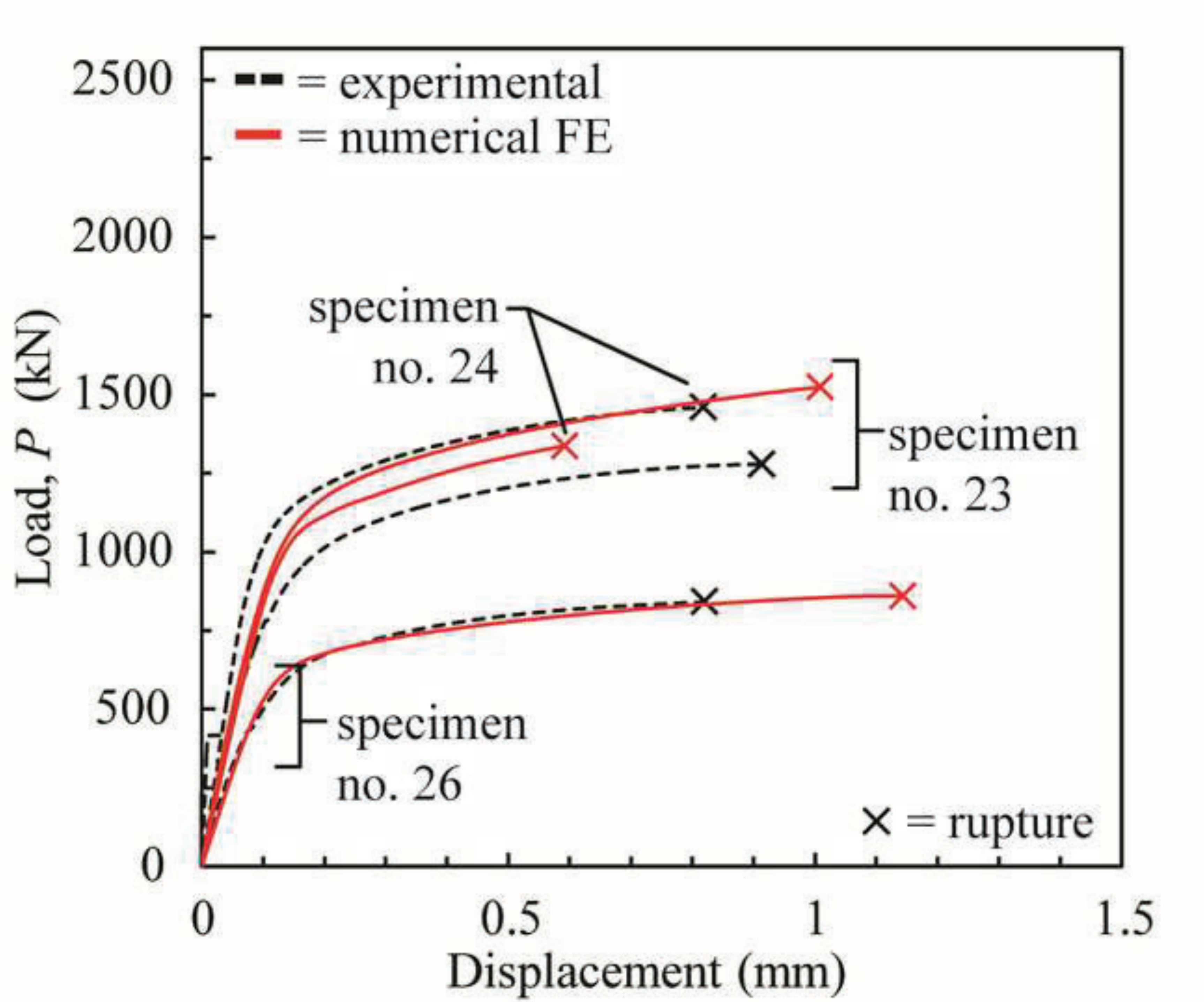
= experimental
= numerical FE
specimen no. 24
specimen no. 23
specimen no. 26
× = rupture
Load, P (kN)
Displacement (mm)
2500
2000
1500
1000
500
0
0
0.5
1
1.5

Figure12b

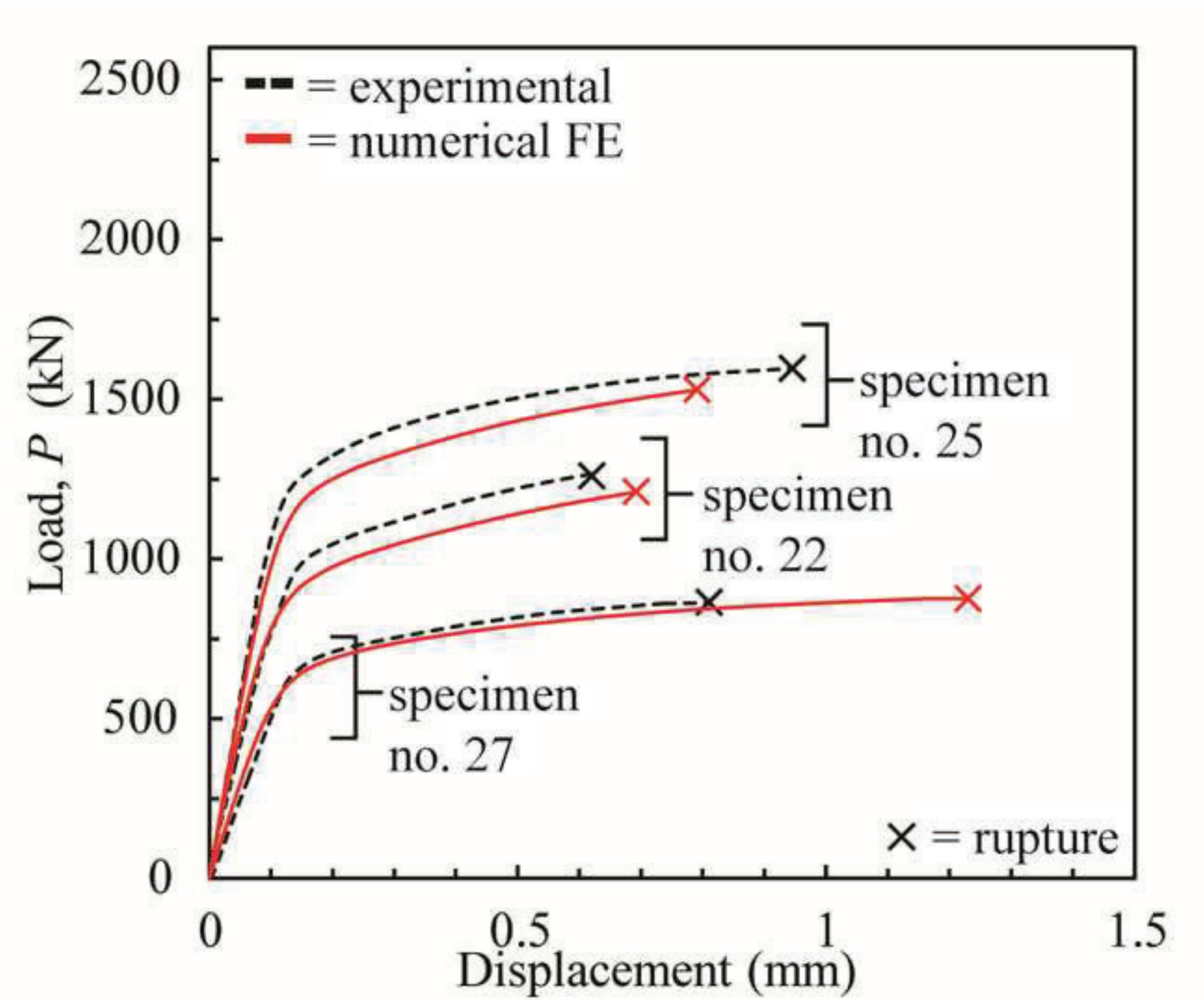

= experimental
= numerical FE
Load, P (kN)
2500
2000
1500
1000
500
0
0
0.5
1
1.5
Displacement (mm)
specimen no. 25
specimen no. 22
specimen no. 27
× = rupture

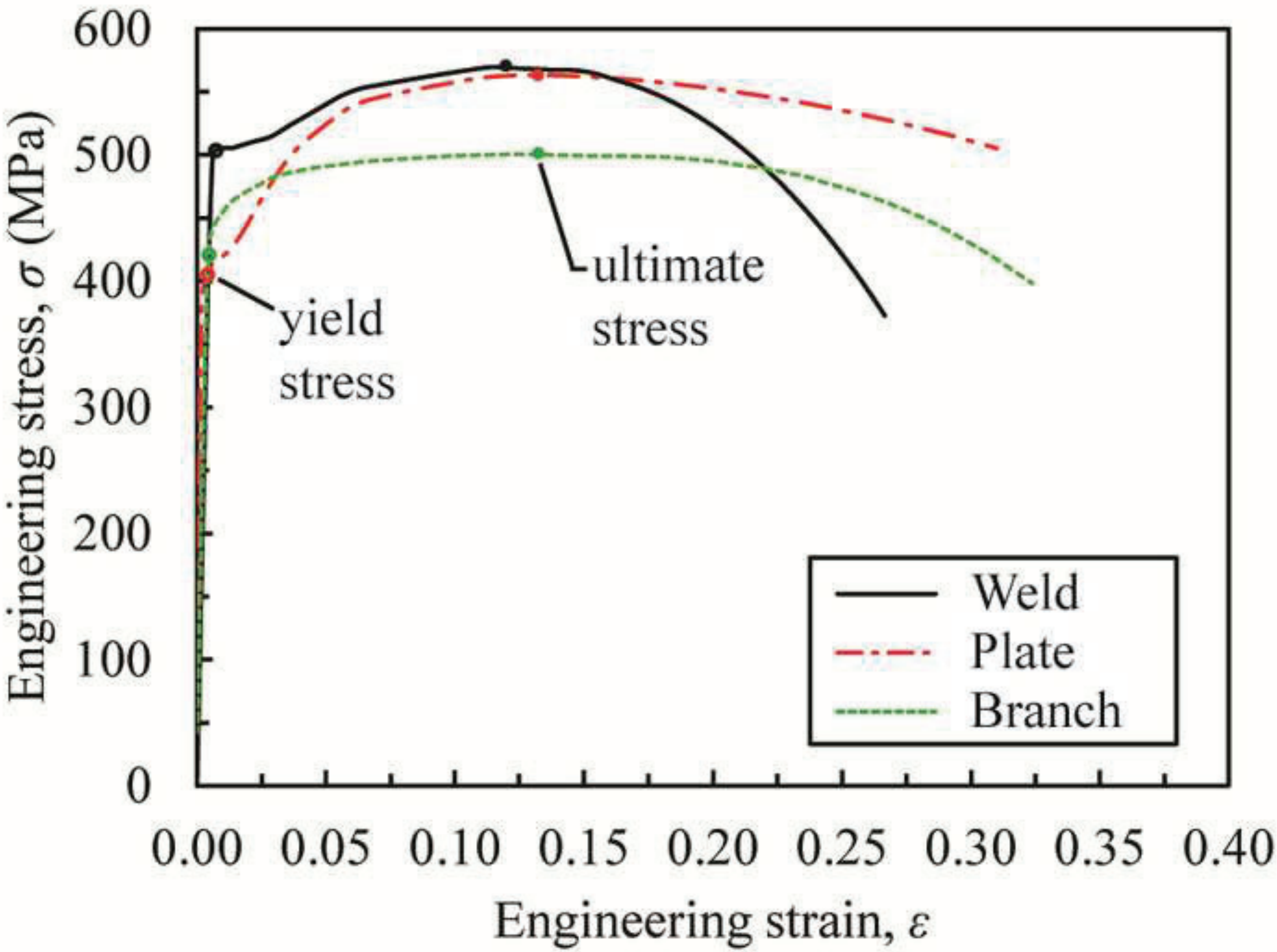
600
500
400
300
200
100
0
Engineering stress, σ (MPa)
yield
stress
ultimate
stress
Weld
Plate
Branch
0.00
0.05
0.10
0.15
0.20
0.25
0.30
0.35
0.40
Engineering strain, ε

Figure14a

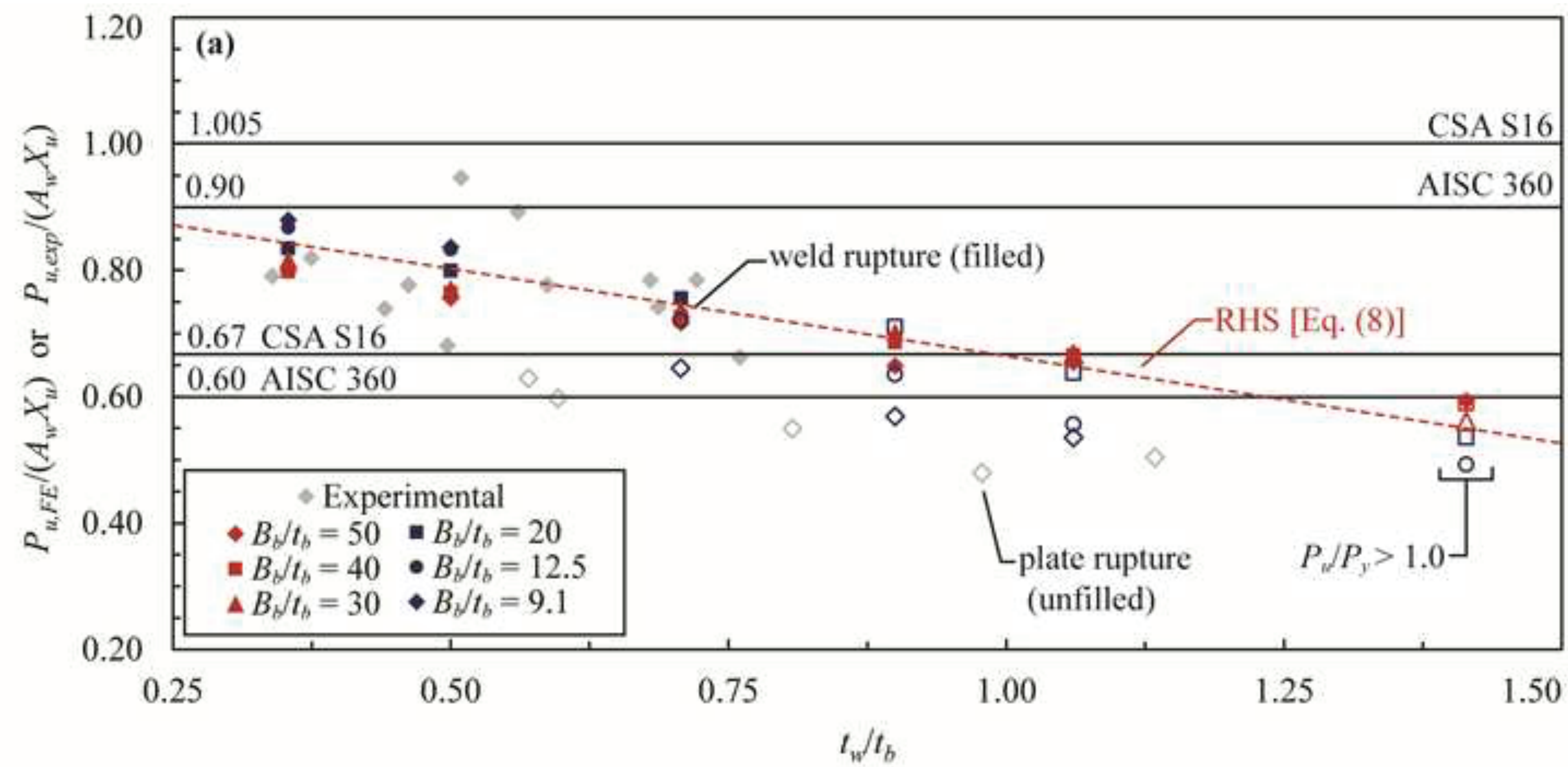

(a)
1.005
CSA S16
0.90
AISC 360
0.67 CSA S16
0.60 AISC 360
weld rupture (filled)
RHS [Eq. (8)]
plate rupture
(unfilled)
$P_u/P_y > 1.0$
Experimental
$B_b/t_b = 50$
$B_b/t_b = 40$
$B_b/t_b = 30$
$B_b/t_b = 20$
$B_b/t_b = 12.5$
$B_b/t_b = 9.1$
$P_{u,FE}/(A_w X_u)$ or $P_{u,exp}/(A_w X_u)$
t_w/t_b
0.20
0.40
0.60
0.80
1.00
1.20
0.25
0.50
0.75
1.00
1.25
1.50

Figure14b

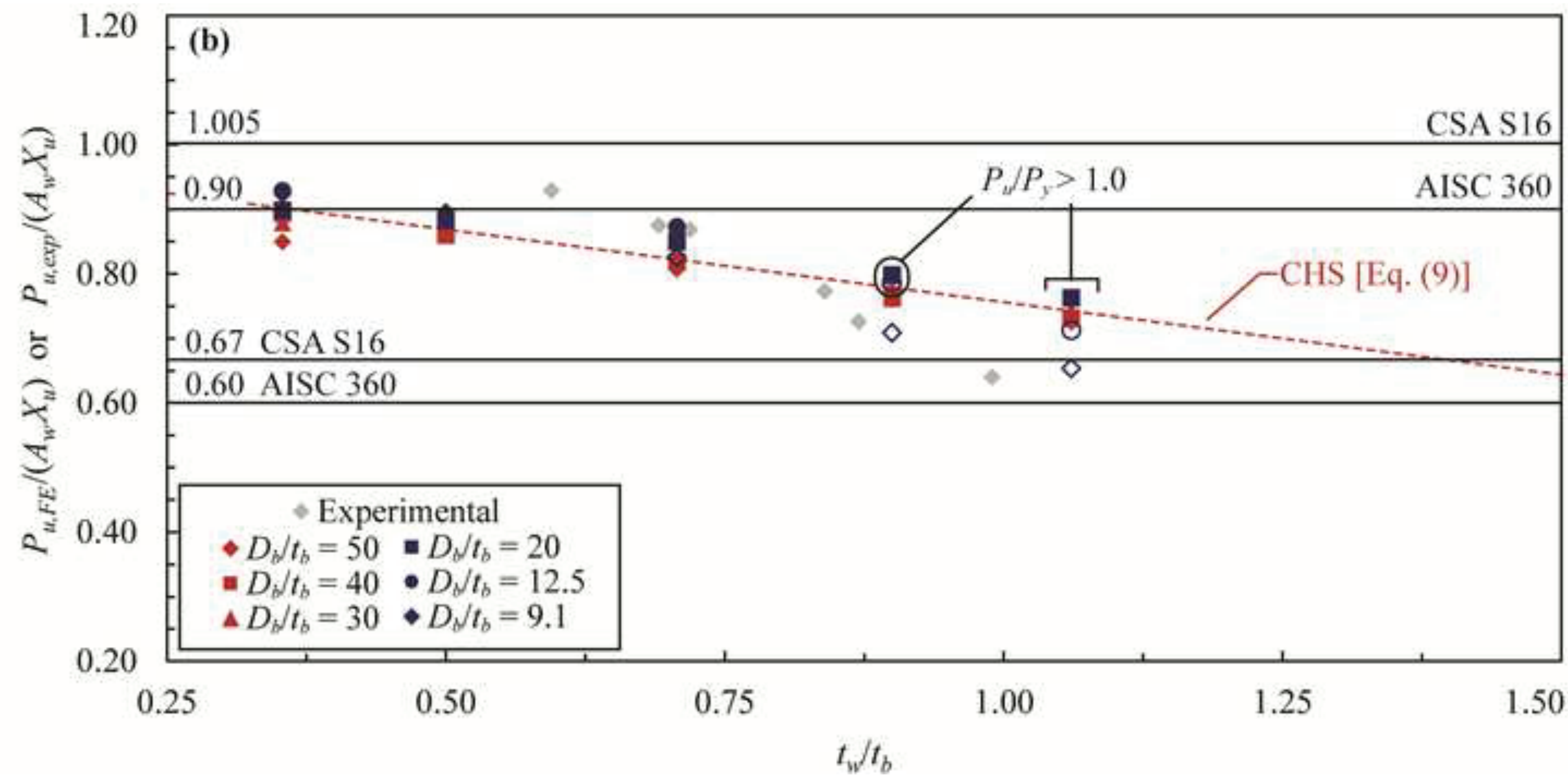
(b)
1.005
CSA S16
0.90
AISC 360
$P_u/P_y > 1.0$
CHS [Eq. (9)]
0.67 CSA S16
0.60 AISC 360
Experimental
$D_b/t_b = 50$
$D_b/t_b = 40$
$D_b/t_b = 30$
$D_b/t_b = 20$
$D_b/t_b = 12.5$
$D_b/t_b = 9.1$
$P_{u,FE}/(A_wX_u)$ or $P_{u,exp}/(A_wX_u)$
1.20
1.00
0.80
0.60
0.40
0.20
0.25
0.50
0.75
1.00
1.25
1.50
t_w/t_b

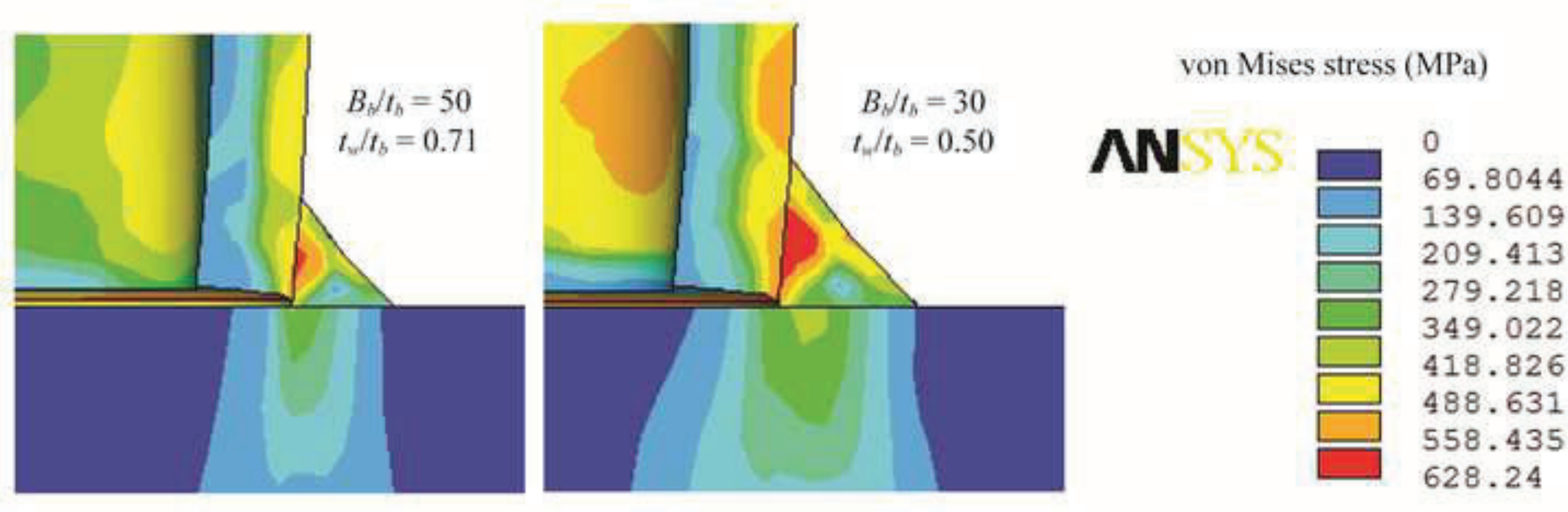

$B_b/t_b = 50$
$t_w/t_b = 0.71$
$B_b/t_b = 30$
$t_w/t_b = 0.50$
von Mises stress (MPa)
ANSYS
0
69.8044
139.609
209.413
279.218
349.022
418.826
488.631
558.435
628.24

Figure16a

Click here to download Figure Figure16a.tif

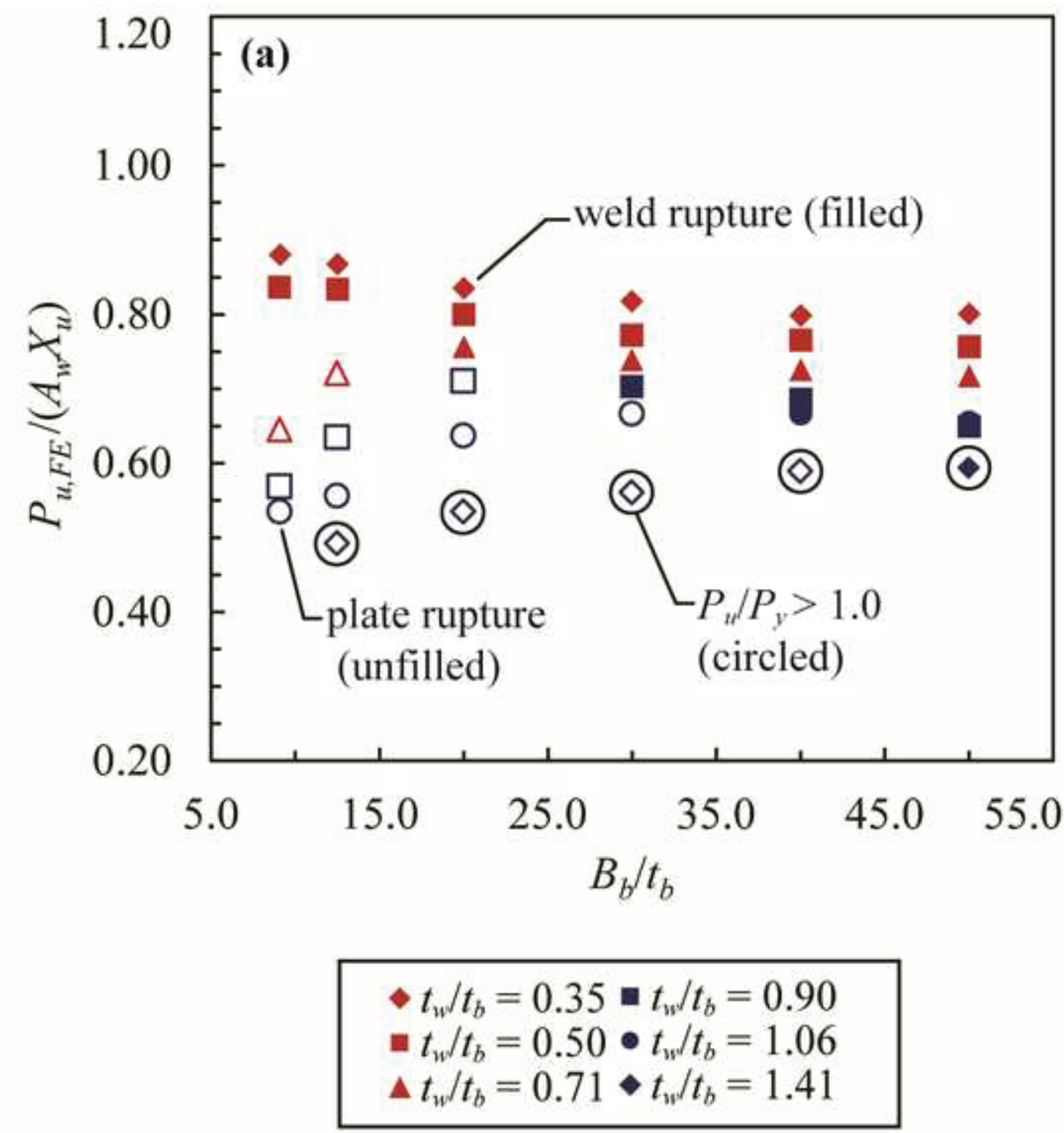

Figure16b

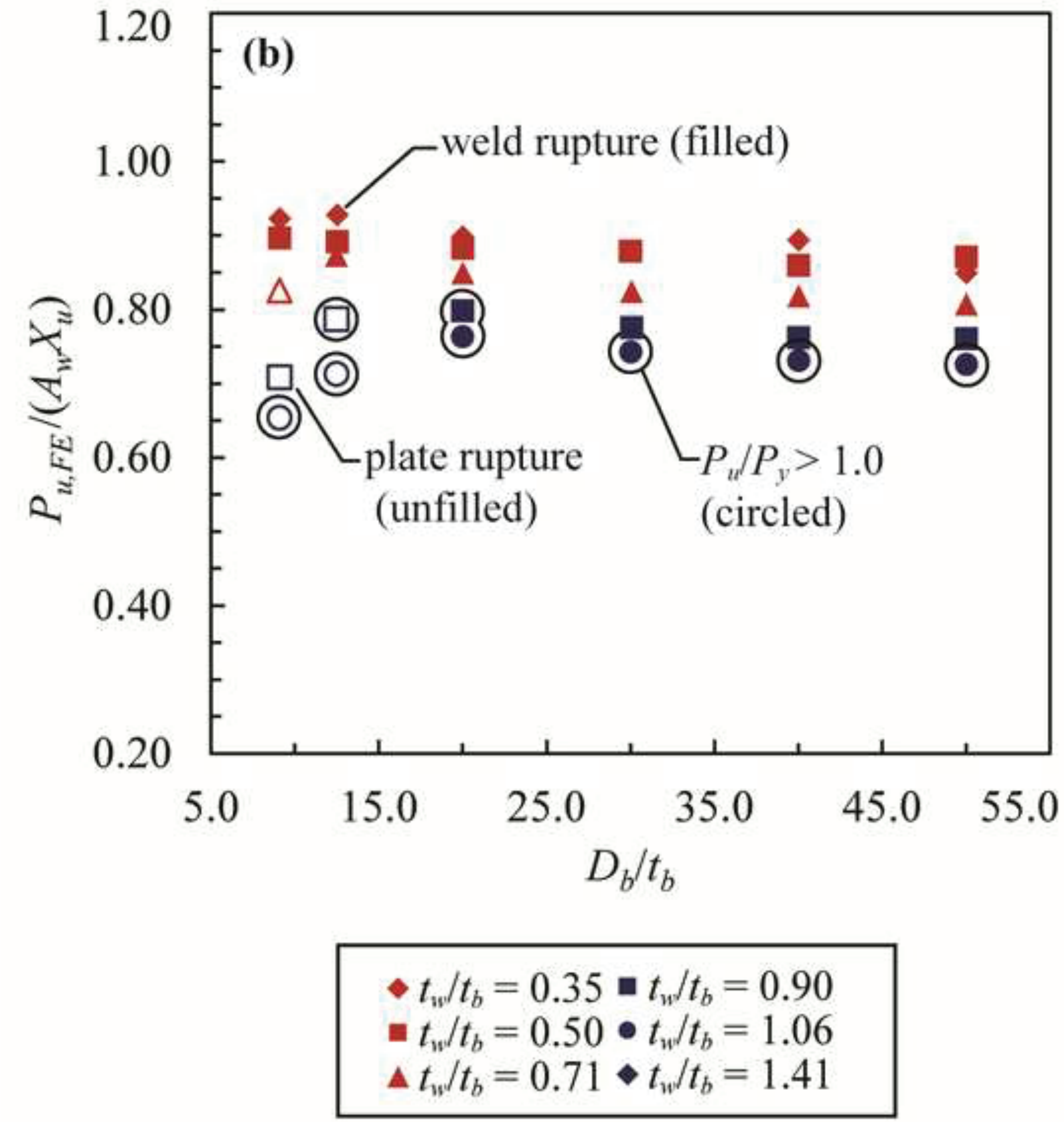

(b)
weld rupture (filled)
plate rupture (unfilled)
$P_u/P_y > 1.0$ (circled)
1.20
1.00
0.80
0.60
0.40
0.20
$P_{u,FE}/(A_wX_u)$
5.0
15.0
25.0
35.0
45.0
55.0
D_b/t_b
$t_w/t_b = 0.35$
$t_w/t_b = 0.50$
$t_w/t_b = 0.71$
$t_w/t_b = 0.90$
$t_w/t_b = 1.06$
$t_w/t_b = 1.41$

Figure17

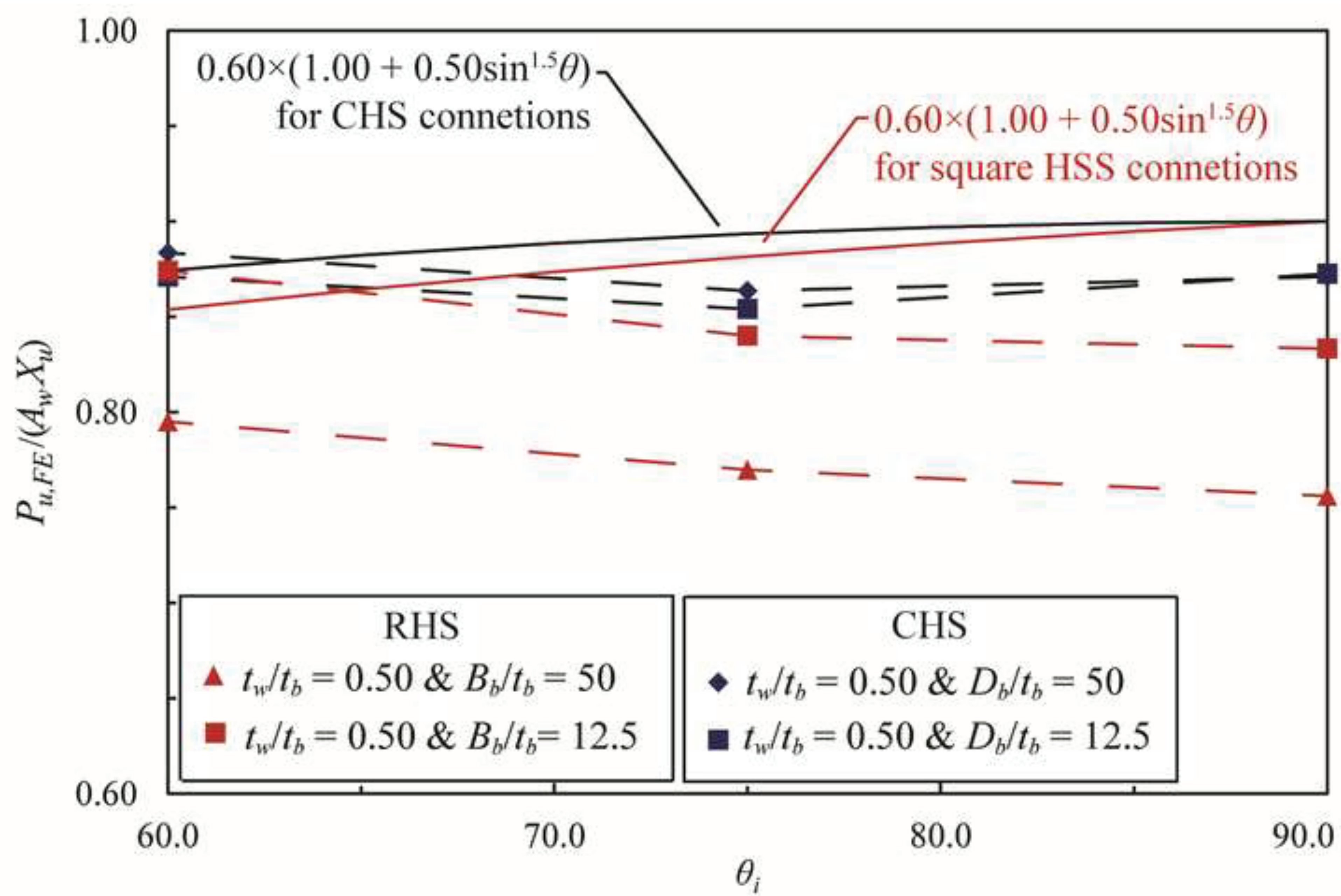

1.00
0.80
0.60
$P_{u,FE}/(A_w X_u)$
$0.60\times(1.00 + 0.50\sin^{1.5}\theta)$
for CHS connetions
$0.60\times(1.00 + 0.50\sin^{1.5}\theta)$
for square HSS connetions
RHS
$t_w/t_b = 0.50$ & $B_b/t_b = 50$
$t_w/t_b = 0.50$ & $B_b/t_b = 12.5$
CHS
$t_w/t_b = 0.50$ & $D_b/t_b = 50$
$t_w/t_b = 0.50$ & $D_b/t_b = 12.5$
60.0
70.0
80.0
90.0
θ_i

Figure18a

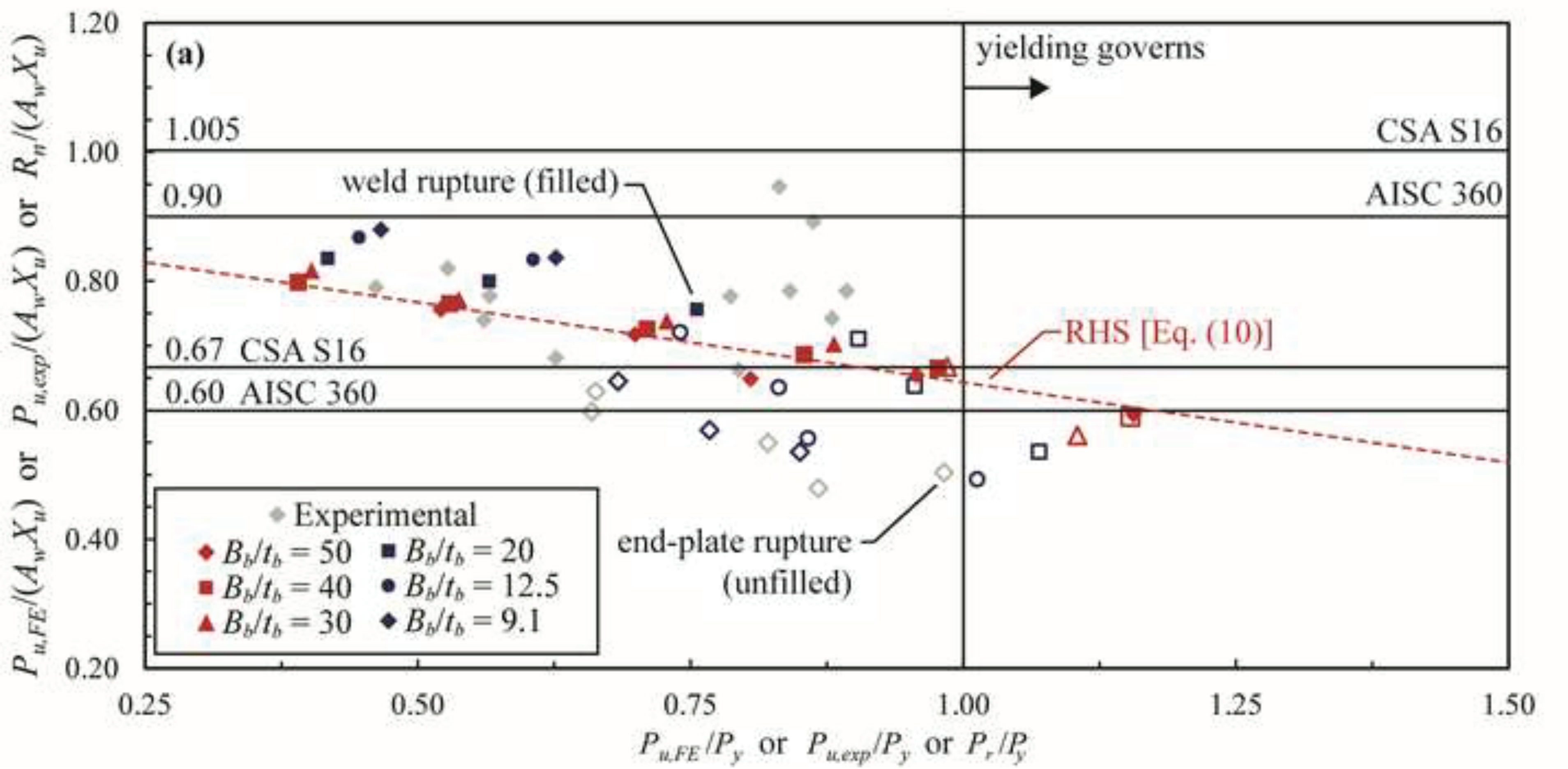

(a)
yielding governs
1.005
CSA S16
0.90
AISC 360
weld rupture (filled)
0.67 CSA S16
0.60 AISC 360
RHS [Eq. (10)]
end-plate rupture (unfilled)
Experimental
$B_b/t_b = 50$
$B_b/t_b = 40$
$B_b/t_b = 30$
$B_b/t_b = 20$
$B_b/t_b = 12.5$
$B_b/t_b = 9.1$
1.20
1.00
0.80
0.60
0.40
0.20
0.25
0.50
0.75
1.00
1.25
1.50
$P_{u,FE}/(A_w X_u)$ or $P_{u,exp}/(A_w X_u)$ or $R_n/(A_w X_u)$
$P_{u,FE}/P_y$ or $P_{u,exp}/P_y$ or P_r/P_y

Figure18b

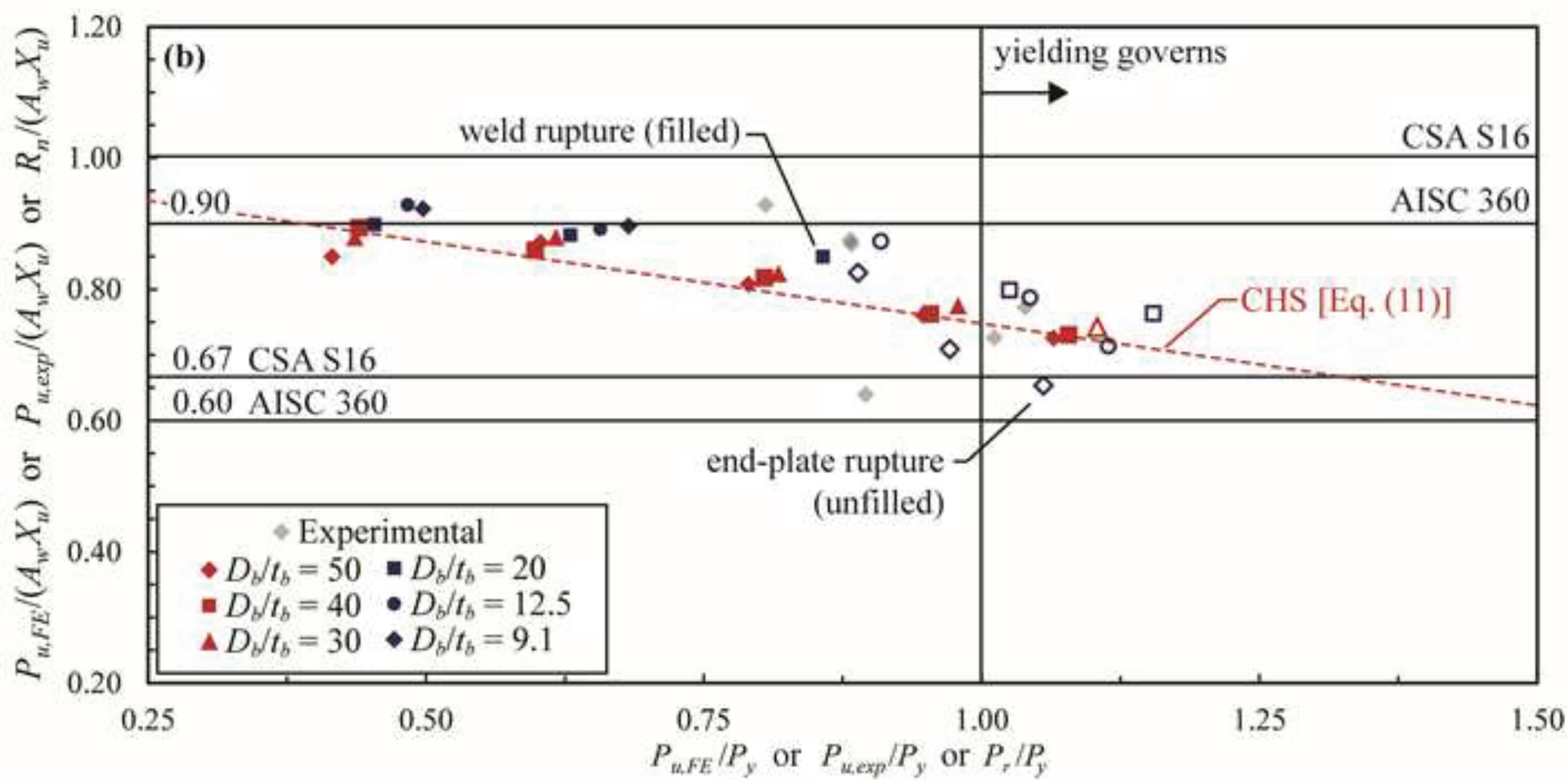

(b)
yielding governs
weld rupture (filled)
CSA S16
AISC 360
0.90
CHS [Eq. (11)]
0.67 CSA S16
0.60 AISC 360
end-plate rupture
(unfilled)
Experimental
$D_b/t_b = 50$
$D_b/t_b = 40$
$D_b/t_b = 30$
$D_b/t_b = 20$
$D_b/t_b = 12.5$
$D_b/t_b = 9.1$
1.20
1.00
0.80
0.60
0.40
0.20
0.25
0.50
0.75
1.00
1.25
1.50
$P_{u,FE}/P_y$ or $P_{u,exp}/P_y$ or P_r/P_y
$P_{u,FE}/(A_w X_u)$ or $P_{u,exp}/(A_w X_u)$ or $R_n/(A_w X_u)$